LBL-36619
UC-404

Lawrence Berkeley Laboratory
UNIVERSITY OF CALIFORNIA

Engineering Division

Advanced Far Infrared Detector and Double Donor Studies in Ge

C.S. Olsen
(M.S. Thesis)

December 1994

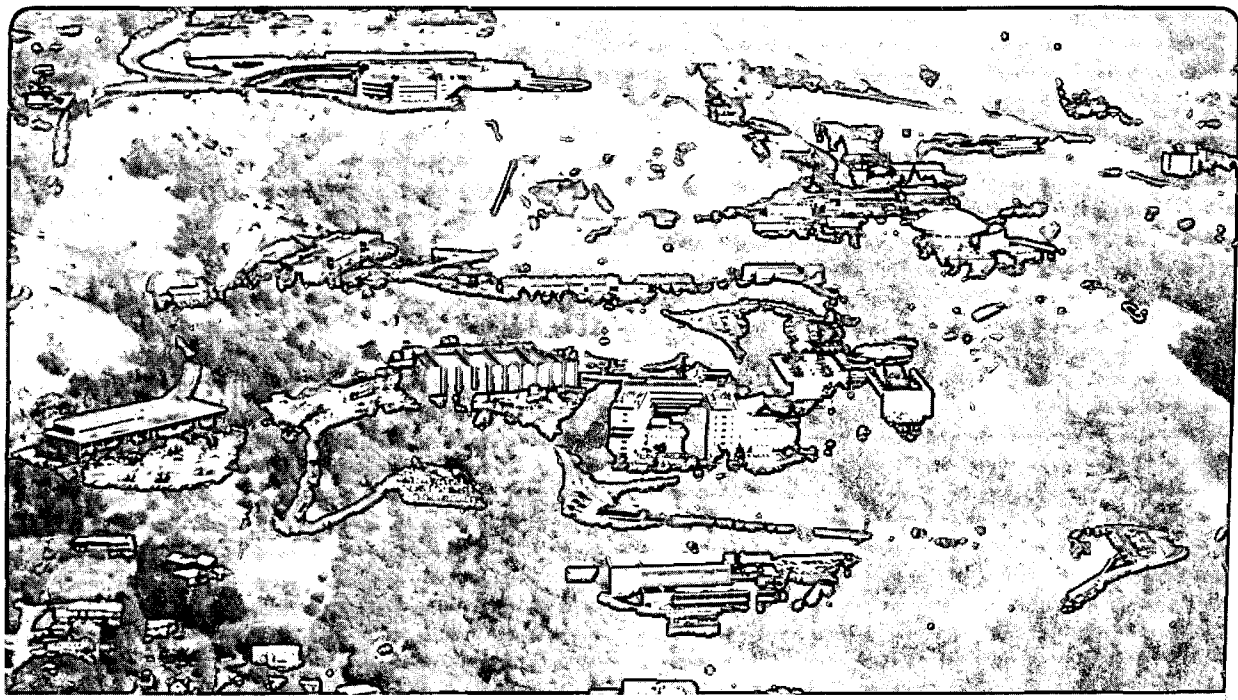

REFERENCE COPY
Does Not
Circulate
Bldg. 50 Library.
LBL-36619
Copy 1

Prepared for the U.S. Department of Energy under Contract Number DE-AC03-76SF00098

DISCLAIMER

This document was prepared as an account of work sponsored by the United States Government. While this document is believed to contain correct information, neither the United States Government nor any agency thereof, nor the Regents of the University of California, nor any of their employees, makes any warranty, express or implied, or assumes any legal responsibility for the accuracy, completeness, or usefulness of any information, apparatus, product, or process disclosed, or represents that its use would not infringe privately owned rights. Reference herein to any specific commercial product, process, or service by its trade name, trademark, manufacturer, or otherwise, does not necessarily constitute or imply its endorsement, recommendation, or favoring by the United States Government or any agency thereof, or the Regents of the University of California. The views and opinions of authors expressed herein do not necessarily state or reflect those of the United States Government or any agency thereof or the Regents of the University of California.

LBL-36619
UC-404

Advanced Far Infrared Detector and Double Donor Studies in Ge

Christopher Sean Olsen
M.S. Thesis

Material Science and Mineral Engineering Department
University of California

and

Engineering Division
Lawrence Berkeley Laboratory
University of California
Berkeley, California 94720

December 1994

This work was supported by U.S. NASA Contract W17605 and A59513CBVC through interagency agreement with the U.S. Department of Energy under Contract No. DE-AC03-76SF00098.

Advanced Far Infrared Detector and Double Donor Studies in Ge

by

Christopher Sean Olsen

B. S. (University of California, Los Angeles) 1991

A thesis submitted in partial satisfaction of the

requirements for the degree of

Masters in Science

in

Engineering-Materials Science & Mineral Engineering

in the

GRADUATE DIVISION

of the

UNIVERSITY OF CALIFORNIA at BERKELEY

Committee in charge:

Professor Eugene E. Haller
Professor Timothy Sands
Professor Nathan W. Cheung

Table of Contents

I. Germanium Blocked Impurity Band (BIB) Far Infrared Detector

1. Introduction 1
    1.1 Motivation for Far Infrared Detector Development 1
    1.2 Photoconductors 2
        1.2.1 Principles of Operation 2
        1.2.2 Figures of Merit 4
        1.2.3 Review of Present Technology 7
    1.3 BIB Detectors 8

2. Ion Implanted BIB Detectors 11
    2.1 Boron Implanted Detectors 11
    2.2 Planar Boron Implanted Detectors 14
    2.3 Characterization of Boron Implanted Layers 16
        2.3.1 Copper in Ge 17
        2.3.2 Hall Effect 18
        2.3.3 PhotoThermal Ionization Spectroscopy (PTIS) 21
        2.3.4 Activation of the Ion Implanted Layers 23
        2.3.5 Deep Level Transient Spectroscopy (DLTS) 24
        2.3.6 DLTS of Boron Implanted into p-type Ge 29
        2.3.7 DLTS of Boron Implanted into n-type Ge 31

3. Characterization Results for BIB Detectors 34
    3.1 Dark Current-Voltage and Spectral Response Techniques 34
    3.2 Bulk Boron Implanted Detectors 37
        3.2.1 Results for High Energy Boron Implanted BIB Detectors 37
        3.2.2 Results for Low Energy Boron Implanted BIB Detectors 42
    3.3 Planar Boron Implanted BIB Detector Results 44
        3.3.2 Asymmetric Devices 44
        3.3.1 Symmetric Devices 45

4. Discussion 47
    4.1 Small wavenumber response 47
    4.2 Absolute Donor Concentration and Cu Contamination 48
    4.3 Future Studies 51

5. Conclusion 52

II. Double Donor Studies

1. Introduction 53

2. Review of Previous Work 54
    2.1 Doping Techniques 54
        2.1.1 Diffusion & Melt Doping 54
        2.1.2 Neutron Transmutation Doping (NTD) 55
    2.2 Characterization of Energy Levels 60
    2.3 Neutron Damage 62

3. Impurity Identification Through Isotope Engineering 63
    3.1 Growth Small Ge Crystals 63
    3.2 NTD Isotopically Enriched Ge 64
    3.3 Characterization 64
        3.3.1 Deep Level Transient Spectroscopy (DLTS) 64
        3.3.2 Isothermal Annealing Behavior 68
        3.3.3 Absorption Spectroscopy 71

4. Selenium Melt Doped Germanium 72

5. Discussion 74

6. Future Work 74

7. Conclusion 76

III. References 77

IV. Appendices
    Appendix A 80
    Appendix B 82
    Appendix C 84
    Appendix D 86

Acknowledgements

I would like to thank Prof. Nancy Haegel for the research experience which lead to my graduate studies. I am especially grateful to my advisor Prof. Eugene Haller for his support in so many ways. I would also like to thank Prof. Tim Sands and Prof. Nathan Cheung for spending the time to critique my thesis. I graciously thank Jack Walton for use of his laboratory for part of this work.

I believe that a large portion of my graduate education comes from my fellow graduate students in both research and academic studies. All my peers really have made this a wonderful group in which to do my graduate work. I especially regard Kohei Itoh and Oscar Dubon as true mentors. Kristin Duxstad has been a wonderful friend, and I thank her for spending the time to review my thesis. I would also like to acknowledge Jeff Beeman for our discussions and extensive help around the lab. I thank Margaret Ragsdale for always being so helpful.

I would like to thank my family for their love and profound influence on my life. I am very grateful for the love and support of Annalise. I thank all my friends and the community who have brought me to this point.

This work was supported by US NASA Contract W17605 and A59513CBVC through interagency agreement with the US Department of Energy Contract DE-AC03-76SF00098.

I. Germanium Blocked Impurity Band (BIB) Far Infrared Detector

1. Introduction

1.1 Motivation for Far Infrared Detector Development

For astronomers and astrophysicists, the far infrared (IR) spectral range of 50 to 400 cm^{-1}, has valuable information for understanding the universe. In the far IR spectral range, excited atomic and molecular species convey information about the temperature and density of the objects emitting the IR radiation. The IR signal is extremely important, because some objects do not appear in the visible spectrum. This data can provide insight into the mechanisms of star formation, physics of interstellar media, nature of the galactic center, early evolution of galaxies, and properties of primitive solar system material (Pilbratt 1994). To view and image distant stellar objects in the infrared spectrum, telescopes must be fitted with infrared detectors. Imaging of objects can be done by stepping one detector over an area, or an array of detectors can be used simultaneously to map out images.

Unfortunately, the earth's atmosphere strongly absorbs in many regions of the IR spectrum. Telescopes must either be positioned at high altitudes or launched into space for optimal detection. Some telescopes such as the Keck on Mauna Kea in Hawaii are land-based at an altitude close to 14,000 feet. Telescopes can also be brought to high altitudes with balloons or aircraft, such as the Kuiper Airborne Observatory (KAO) operating out of Moffett Field, California. By putting a telescope into orbit, the earth's atmosphere can be avoided entirely. The Infrared Astronomical Satellite (IRAS) was the first IR telescope in space. It was launched in 1983 and catalogued thousands of new infrared sources (Rieke, et al. 1986). The quality of the data collected by IRAS was

partly limited by the sensitivity of the IR detectors. The discoveries, however, were spectacular and have encouraged further space telescope missions and stimulated research into improving far infrared detectors.

There are few detectors which operate in the 50 to 100 cm^{-1} range. Bolometers work in this range, but have poor sensitivity compared to photoconductive detectors. Stressed Ge:Ga detector have good sensitivity in this range, but the mechanical stressing apparatus poses difficulties which will be elaborated on later. This work focused on research and development of a far infrared, boron doped germanium blocked impurity band (BIB) detector that will operate in this range. Several types of other detectors will be discussed to clarify the advantages of BIB detectors over other detectors.

1.2 Photoconductors

1.2.1 Principles of Operation

Semiconductor IR detectors are often configured as photoconductors. There exists two types of photoconductors. Intrinsic photoconductors are undoped, while extrinsic photoconductors are doped with a specific impurity. They operate by absorbing photons which in turn produce free charge carriers (electrons and/or holes). These carriers can be detected by measuring the conductivity change in the material.

Intrinsic photoconductors operate by the excitation of an electron from the valence band to the conduction band, leaving behind a hole. To make this jump, the electron must receive enough energy to excite it across the band gap, therefore only photons with energies greater than the band gap of the semiconductor are detected. Most semiconductor band gap energies range between 3 eV (blue light, example: ZnSe, GaN)

and 0.3eV (near IR, example: InSb, MCT). $Hg_xCd_{1-x}Te$ alloy (MCT) detectors are often used in the IR because they operate from the near to the mid infrared (1.57 to 0.073eV) depending on the composition of the alloy (x), which changes the band gap energy. The low energy limit for $Hg_xCd_{1-x}Te$ intrinsic photoconductors and photodiodes is due to difficulty controlling the alloy composition at the microscopic level. Therefore, detection in the far IR cannot be obtained with intrinsic photoconductors.

Extrinsic photoconductors function through the photoexcitation of an electron (hole) bound at a donor (acceptor) into the conduction (valence) band. The shallow impurity ionization energy, E, is the energy difference between the 1s-like ground state of the impurity and the band edge. The ionization energy of shallow impurities is much smaller than the band gap, thus they can be used to detect at much longer wavelengths, λ. The relations between E, λ, and ν are given in equation 1.1.

$$\lambda(\mu m) = \frac{10^4}{\nu(cm^{-1})} = \frac{1.24}{E(eV)} \qquad [1.1]$$

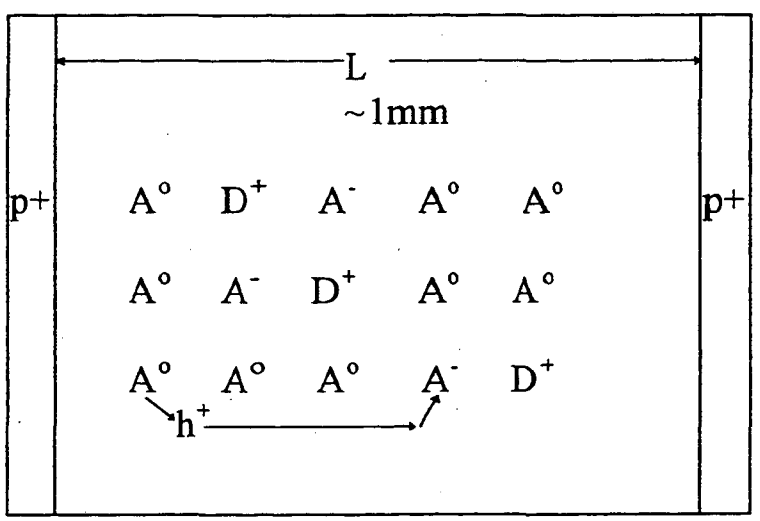

Fig. 1.1 Schematic of extrinsic photoconductor

Shallow impurity ionization energies are small, therefore very low operating temperatures must be used to provide neutral acceptors for photoionization. After a hole is photoionized from a neutral acceptor, A^o, into the valence band, the free hole changes the electrical conductivity. The contribution of the hole to the signal current will depend on the distance it travels in the photoconductor before it returns to another ionized acceptor, shown in Fig 1.1. The ionized acceptor will eventually be neutralized by recombination with another hole. The concentration of ionized acceptors at low temperatures will be mainly determined by the concentration of donors, due to compensation. A high concentration of ionized acceptors will cause the free hole contribution to the conductivity to be much smaller. The change in conductivity is measured with a low noise, electronic amplifier circuit. Degenerately doped contacts are needed to allow holes to enter and exit the device at low temperatures.

The photoconductivity signal must be greater than the noise associated with the photon background and the current flowing through a device under no illumination, the dark current. To minimize the dark current, these extrinsic Ge phoconductors must be operated at extremely low temperatures, $T<4.2K$. In the following specific parameters and figures of merit of photoconductors, such as dark current, responsivity, and noise equivalent power will be discussed.

1.2.2 Figures of Merit

Many parameters are required to fully characterize a photoconductor, such as noise equivalent power (NEP), quantum efficiency, responsivity, spectral response, and dark current. For low level IR studies, a device should have low NEP and high quantum efficiency.

One of the important figures of merit of a detector is its spectral response, which is the strength of the photoconductivity signal at different wavelengths. The spectral response shows in what range a detector can be optimally used. Responsivity is the strength of the detector's signal at a specific wavelength. Responsivity (R) is the ratio of the photoconductive current and the incident photon power, measured in Amps per Watt. A high responsivity is desirable for detecting small signals. The responsivity, R, is affected by many parameters and is a function of wavelength. The definition of responsivity is given in the following equation.

$$R = \frac{e}{h\nu} G\eta \qquad [1.2]$$

In the above equations, e is the electron charge, h is Planck's constant, ν is the frequency of incident photons, η is the responsive quantum efficiency, and G is the photoconductive (PC) gain. This gain is defined as the number of carriers detected divided by the number of carriers produced. The PC gain must be measured indirectly with measurable parameters. The PC gain can be expressed as the ratio of the free carrier lifetime, τ, over the transit time, t, shown in equation 1.3. The transit time is the drift velocity, v_{drift}, divided by the device length, L. The drift velocity is mobility, μ, times the voltage V divided by L. We now can write equation 1.3:

$$G = \frac{\tau}{t} = \tau\mu \frac{V}{L^2} \qquad [1.3]$$

The responsivity can then be written

$$R = \frac{eV}{h\nu L^2} \eta\tau\mu \qquad [1.4]$$

Responsive quantum efficiency is defined as the ratio of photons absorbed to photons incident upon the device. Responsivity has been discussed by many authors (Bratt 1977; Haegel 1983; Haller 1985).

The spectral response of a photoconductor has a sharp onset at the ionization energy E_{ion} of the impurity (Figure 1.2). The photoconductive response for a detector doped with shallow, hydrogenic center rises to a maximum when the transition from the ground state is direct to the valence band edge maximum. With increasing photon energy, the transition to the valence band shifts away from the valence band top in k-space and the ground state wavefunction amplitude rapidly drops. Because of this, the response decreases at energies greater than the ionization energy with $E^{2/3}$.

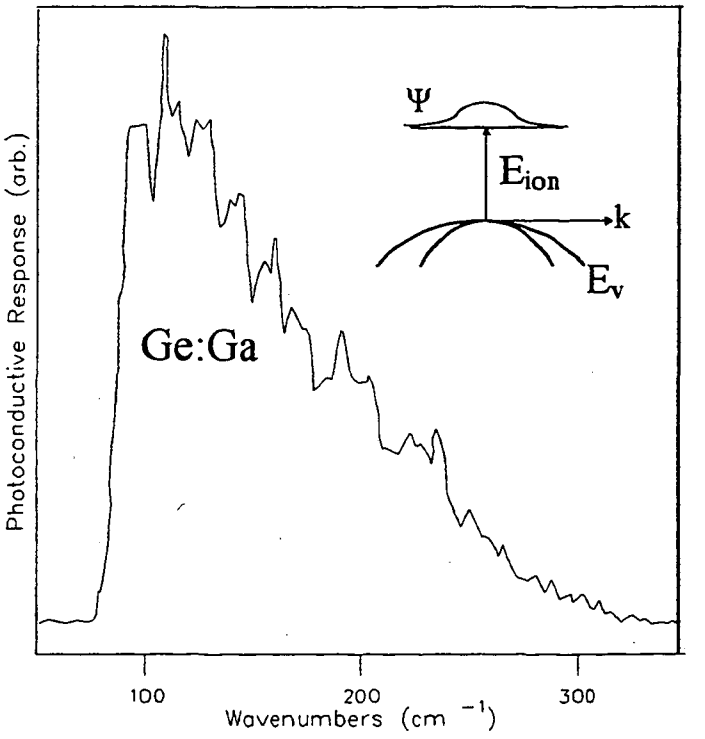

Figure 1.2 Photoconductivity of Ge:Ga crystal 113

Another important parameter used to characterize photoconductive detectors is the Noise Equivalent Power (NEP). NEP is defined as the power required to produce signal to noise ratio of one per unit bandwidth.

$$NEP = \frac{P}{S/N} \qquad [1.5]$$

In the above equation, P is the signal power (W), S is the signal (A), and N is the background noise (A/√Hz) (Haegel 1983). NEP values as low as 10^{-16} W/√Hz to 10^{-18} W/√Hz are typical for the best far IR Ge:Ga photoconductors.

1.2.3 Present Technology

Germanium extrinsic photoconductors are well suited for far IR detection, because they have impurity ionization energies from 10meV(80cm^{-1}) to 50 meV(400cm^{-1}) (Bratt 1977). Germanium detectors doped with gallium (Ge:Ga) respond from 83 cm^{-1} to 250 cm^{-1}. Ge:Ga detectors are operated at T=3.0 K to minimize the noise. The quantum efficiency is about 0.04, and the responsivity is typically 3 A/W at ν=111 cm^{-1} for concentrations [Ga]=10^{14} cm^{-3} and N_D=10^{12} cm^{-3} (Haegel 1983).

Silicon is better suited for mid IR detection because its shallow dopants are between 4 to 6 times deeper than Ge (Sclar 1976). However in GaAs typical hydrogenic donors have ionization energies as shallow as 6 meV such as silicon and sulfur(Ozeki, et al. 1977) that can be used to detect as low as low as ~40 cm^{-1}. GaAs photoconductors have not yet been developed.

Germanium can be made to work in the far infrared with uniaxial stress out to ~50 cm^{-1}. Application of uniaxial stress to p-type Ge lowers the acceptor binding energy to ~6meV(48cm^{-1}) (Haller, et al. 1979). Stressed detectors are fragile and are bulkier with

the mechanical stressing rig. They are also subject to fracture during rocket launches. Large area stressed detector arrays are very difficult to develop and detectors not requiring mechanical stress would definitely be preferable. These drawbacks are some of the limitations that have motivated research in the area of germanium blocked impurity band (BIB) detectors. Advantages of BIB detectors over other conventional detectors will be discussed in the following section.

1.3 BIB Detectors

In principle, BIB detectors have several advantages over conventional detectors. Like conventional detectors, BIB detector are operated at very low temperatures, $T < 4.2$ K. They consist of a two layer structure, a heavily doped (IR absorbing) region and a pure (blocking) layer(Fig 1.3 bottom) with degenerately doped contacts. Because the IR absorbing layer is doped to a much higher concentration ($\sim 10^{16}$ cm^{-3} majority shallow impurities, $\sim 10^{12}$ cm^{-3} minority impurities) than conventional photoconductors($\sim 10^{14}$ cm^{-3} majority shallow impurities, $\sim 10^{12}$ cm^{-3} minority impurities), the carrier wavefunctions begin to overlap and exhibit impurity banding. Hopping conduction occurs between the impurities, which would make the dark current high if the blocking layer were not present and the heavily doped layer extended from contact to contact. Banding also increases the width of the impurity energy level and decreases the effective ionization energy. For shallow levels in Ge, a decrease in the ionization energy begins to occur at 5×10^{15} cm^{-3} and a doping concentration above 3×10^{17} cm^{-3} results in a degenerate metallically conducting layer. This decrease in ionization energy provides a photoconductive response at extended wavenumbers, a desirable property for many photodetector applications. A

further advantage of the BIB detector is that a smaller detector volume is needed for efficient absorption. The high doping provides increased photon absorption. The reduced detector volume decreases the interference of cosmic radiation "hits" with device operation. Cosmic radiation produces a large concentration of electron-hole pairs that saturate electronics. A third advantage is that a BIB device has unity gain, i.e., every photoinduced charge fully crosses the device once. The principle of operation will be discussed below in further detail.

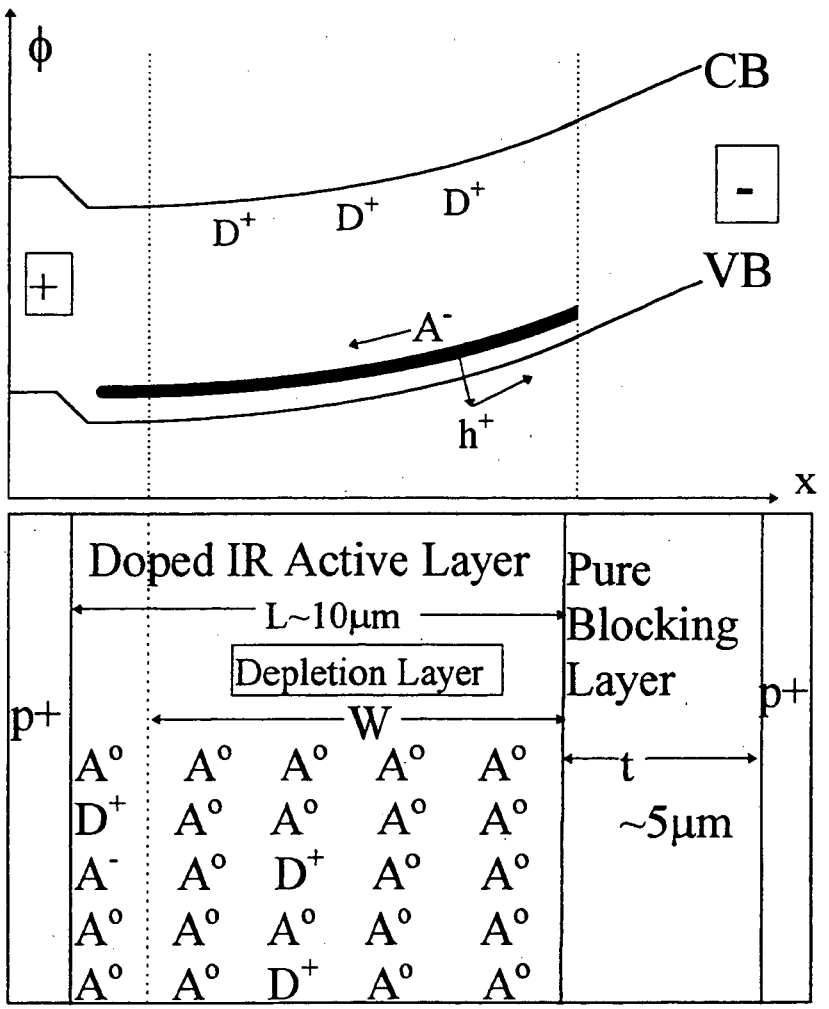

Figure 1.3 top) Potential Energy ϕ for a reverse biased BIB detector bottom) Schematic of reverse biased BIB detector relative to top diagram

The application of a bias to a BIB detector creates a depletion layer, similar to a depletion layer in a p-n junction. In a p-n junction, the depletion layer is devoid of free carriers and contains fixed ionized acceptors and donors. Unlike in a p-n junction, the depletion layer in a p-type BIB is devoid of ionized acceptors in the depletion layer. Hopping conduction in the impurity band allows ionized acceptor states to move to the positively biased contact via holes traveling through the impurity levels. A p-type BIB detector is shown with a negative bias on the blocking layer side in Fig. 1.3.

When the bias is first applied, holes are injected from the positively biased contact into the doped layer. The holes travel through the impurity level and fall onto the ionized acceptors. Thus, the negative acceptor states, not the actual impurities, are swept out towards the positively biased contact. In the depletion layer, the only ionized species are the donors, shown in Fig. 1.3 top.

When a photon excites a hole inside the depletion layer into the valence band, this free carrier travels through the depletion layer and the blocking layer in the valence band to the negatively charged contact. The negative acceptor state A^- propagates via hopping of holes from neighboring neutral acceptors all the way to the positive electrode. We see that independent of the location of the photoionization event, one charge travels all the way from one contact to another. The collection of both the hole and the ionized acceptor state results in unity gain.

Similar to a single-sided p-n junction, the width of the depletion layer depends on the donor concentration and the applied voltage, which is derived from Poisson's equation. Petroff and Stapelbroek(Petroff and Stapelbroek 1984) included the blocking layer thickness dependence, shown in equation 1.6.

$$W = \sqrt{\left[\frac{2\varepsilon\varepsilon_o(V_a - V_{bi})}{eN_d} + t^2\right]} - t \qquad [1.6]$$

In the above equation, $\varepsilon\varepsilon_o$ is the dielectric constant, V_a the applied bias, V_{bi} the built in voltage, N_d the minority doping concentration, and t the blocking layer thickness. Depletion of a BIB detector is important because the positive ionized donors produce the charge collection field. Photons are only collected from the depleted part of the IR absorbing layer, so large depletion widths are an advantage.

The operation of a BIB detector in forward bias also yields some signal. Holes are injected from the positively biased contact (negative in Fig. 1.3) into the pure blocking layer and travel to the doped layer, where they fall into ionized acceptors. The holes become trapped by the ionized acceptors because the acceptor level is the lowest energy for the holes. At low temperatures, the hole is not thermally excited back into the valence band. When a photon impacts the device, a hole is excited into the valence band and travels to the negatively charged contact, while the A^- state moves some distance to the edge of the depletion layer. Even though the forward bias shows some photoresponse it is obviously not the optimal polarity, because at higher biases, the dark current increases, similar to a p-n junction.

2. Ion Implanted BIB Detectors

2.1 Boron Implanted Ge BIB Detectors

A BIB detector requires the creation of an ultra-pure layer on a heavily doped layer. Si BIB detectors are made by epitaxial growth of an ultra-pure blocking layer on

top of the IR active layer. Efforts to epitaxially grow the necessary layers for Ge BIB detectors have had very limited success. Because of the much larger Bohr orbits of the shallower dopants, the impurity concentration of the pure and IR active layers must be a factor of 100 smaller in Ge BIB detectors compared to Si BIB detectors. There are many difficulties with Ge epitaxial growth, such as impurity spikes at the interface between the pure blocking layer and the IR active layer. Contamination at the high growth temperatures (typically 750°C) has also not been resolved. Due to these persistent problems with epitaxial growth, I.C. Wu produced the first implanted BIB detectors by implanting boron in ultra-pure germanium (Wu, et al. 1991). Ion implantation provides a controllable method for introducing dopants into ultra pure germanium. Control of the depth of the dopant is fixed by the energy used and the concentration is fixed by the dose of ions. The ion implantation fabrication method avoids the growth problems. The major limitations of this technique are the introduction of lattice damage, the activation of defects in the material, and the rather limited depth of standard ion implantation. Some of the Ge BIB detectors produced by Wu showed response to $55cm^{-1}$, but they had rather low responsivity figures (Wu, et al. 1991).

The irreproducibility in long wavelength response suggests that the IR active layers were not depleted during device operation. A large minority concentration, N_D, would limit the depletion width of the boron implanted IR active layer. Attempts to pinpoint the nature and concentration of such donors have not been successful.

Figure 2.1 is a schematic of an ion implanted BIB detector. It is important for a BIB detector to have a small blocking layer thickness to maximize the depletion of the IR active layer for a given bias. Ion implantation energies are limited, therefore boron can

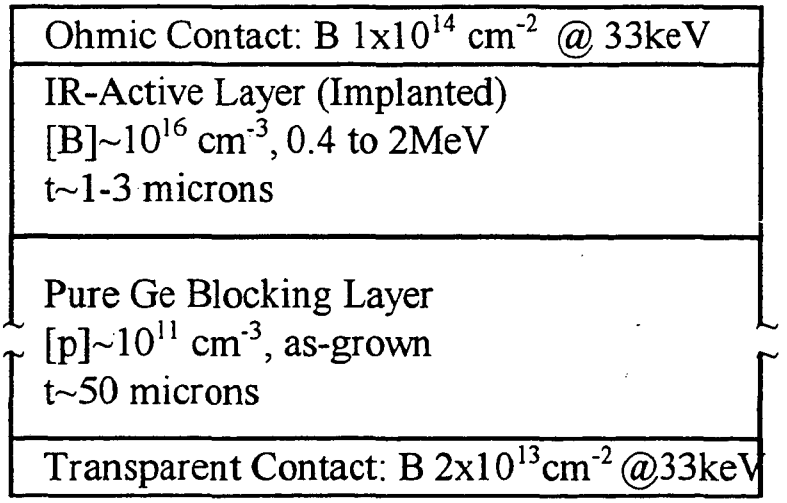

Fig. 2.1 Ion Implanted BIB Detector

only be implanted to several microns deep. As a consequence, the majority of the substrate thickness is ultra pure and acts as a blocking layer. It is possible to reduce the thickness of the blocking layer by chemical and mechanical means, however the mechanical rigidity of the device must be maintained. The minimum practical thickness lies between 30 and 50 μm for a 3 mm by 3 mm device. With the blocking layer this thick, it is difficult to obtain acceptable depletion layer widths at voltages before breakdown occurs. Breakdown occurs when a carrier acquires sufficient energy to impact ionize other neutral impurities. The process multiplies and large currents are generated. The dependence of the depletion width on blocking layer thickness and voltage is shown in Fig. 2.2.

The process used to fabricate ion implanted Ge BIB detectors is described in detail in Appendix A. Even though the ion implanted Ge BIB detector has limitations, it was the only working Ge BIB device, before the development of the planar ion implanted BIB.

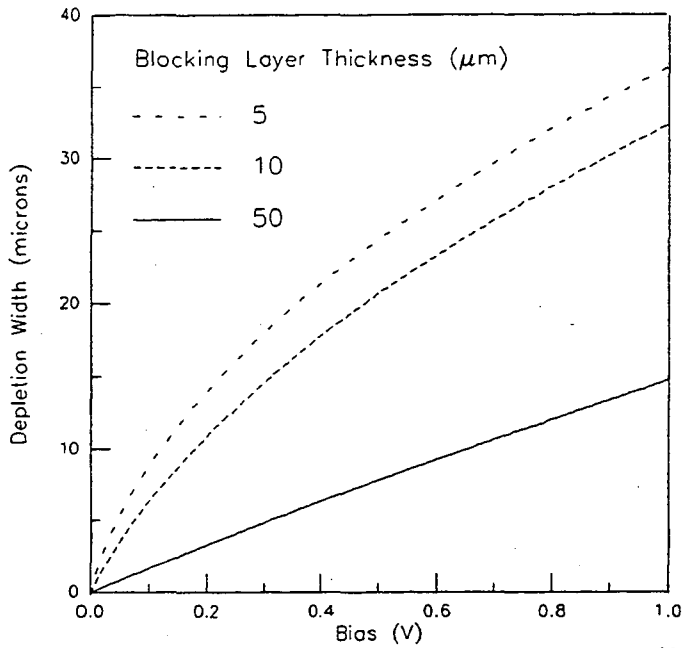

Fig. 2.2 Depletion Width of BIB Detector with $N_D=10^{12}$ cm^{-3}.

2.2 Planar Boron Implanted BIB Detectors

To overcome the disadvantages of the thick blocking layer of the implanted BIB, an idea was developed to move the contact, IR absorbing, and blocking regions of the BIB detector onto the surface of a wafer, making the device planar. An advantage of this device is the complete control of the blocking layer width and the IR active layer width. The control of the geometric structure of the device allows manipulation of the depletion width of the device and ultimately the photoresponse of the device. Blocking layer widths should be about 5 μm for Ge BIB detectors to maximize depletion, shown if Fig. 2.2. The vertical depth of the device is determined by the ion implantation energy. Fabrication of the planar device requires photolithography to define and control the width of the implanted IR absorbing region and the blocking region.

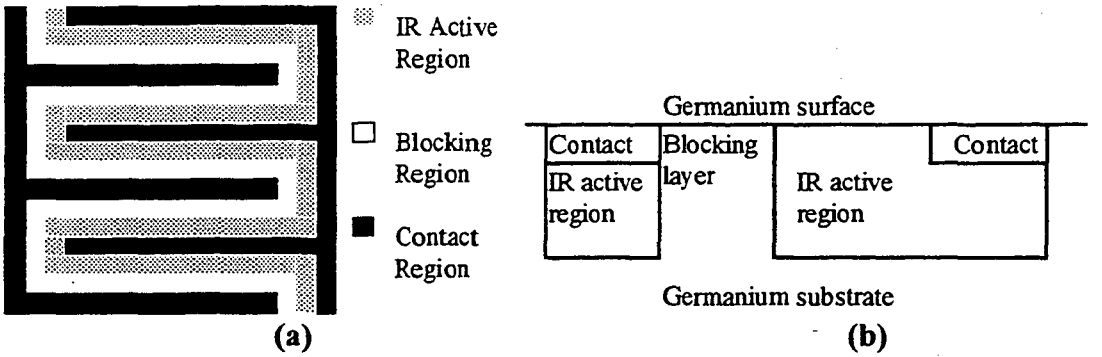

Fig. 2.3 (a) Plane view of Planar Ion Implanted BIB Detector.
(b) Cross sectional view of implants into Ge surface.

Another advantage is that ion implantation allows precise control of the shallow impurity concentration, which affects the response at short wavenumbers. The vertical depth and concentration determine the absorption of the IR active layer. A schematic of a planar ion implanted BIB structure is shown in figure 2.3.

Because of the implantation sequence to be described later, the IR active region is implanted next to and underneath the contact structure. The IR active region under the contact will not hinder the device, but may actually absorb photons which are scattered in the device. A disadvantage of this device is that the depth is limited to 1 to 3 μm. This puts a limit on the absorption which can be attained. Another disadvantage is that ion implantation is known to produce defects which may hinder the device performance.

The fabrication of a planar BIB detector requires at least 2 photolithography steps. One step delineates the contacts and the other the IR absorbing region. A third photolithography step was added to simplify electrical connection of the devices after the implantation and annealing.

The unimplanted portions of the device (blocking region) need a masking material that will stop the boron ion beam during implantation. A masking material had to be chosen for high energy implantation. The requirements for a good implantation mask are high atomic mass, high sputter deposition rate, low solubility in Ge, and an ability to remove the mask from the Ge without damaging the surface. Many materials were considered to find the best mask. Photoresist has a low atomic mass and polymerizes during high energy implants, which may make it difficult to remove. Gold cannot be removed without damage to the surface, titanium has a very low sputtering yield, and aluminum has a low atomic mass. Silver appears to satisfies all of the requirements for a implantation mask and was used for this work.

The process used to fabricate planar boron implanted Ge BIB detectors is described in detail in Appendix B.

2.3 Characterization of Boron Implanted Layers

Note: Germanium wafers are referred to by two numbers, such as 730-10.1. The first number 730 refers to the crystal boole from which the wafer was cut. The second number 10.1 is the distance in cm from the seed of the crystal.

Before fabrication of BIB detectors, the boron implanted layers were characterized. Ion implantation of boron into Ge creates damage, so that the Ge must be annealed to remove deep level defects as well as to activate hopefully all the boron. To measure the degree of activation of boron, Hall effect measurements were used to determine the sheet concentration. Variable temperature Hall effect (VTHE) measures not only concentrations, but it also allows the determination of the energy levels of

shallow impurities. Shallow levels were identified with Photothermal Ionization Spectroscopy (PTIS) and deep levels were characterized by Deep Level Transient Spectroscopy (DLTS). Background information of Cu in Ge will be discussed, because Cu can be an important contaminant in the implanted layer.

2.3.1 Copper in Ge

Copper diffuses interstitially in Ge which means it can diffuse rapidly and is one of the most common contaminants. Copper's substitutional concentration is much higher than its interstitial concentration for temperatures above 450°C (Hall and Racette 1964). Copper on a substitutional Ge site is a triple acceptor. The acceptor levels of substitutional Cu are at E_v+44meV, E_v+330meV, and E_c-265meV (Woodbury and Tyler 1957). Fuller and Severiens did radioactive tracer measurements with ^{64}Cu in Ge and showed that at high temperatures Cu is a positive ion and must be a donor when interstitial, Cu_i (Fuller and Severiens 1954). No information on the energy level of Cu_i donor has been published. The stability and solid solubility of the Cu_i may be very low at room temperature, explaining why it is has never been directly observed.

Many studies show that there must exist large concentrations of electrically inactive Cu in some Ge crystals. Such Cu is passivated in the CuH_3 state. The CuH_2 complex has been studied in great detail with spectroscopy, uniaxial stress, and H isotope substitution. It has been found to be a single acceptor with a broad manifold of the ground components near 17 meV above the valence band (Kahn 1986). The CuH complex has been studied with DLTS and is a double acceptor with levels of 67 and 195 meV above the valence band top (Zach 1992). A further discussion on Cu will be presented in a later chapter.

2.3.2 Hall Effect

Variable temperature Hall effect is one of the most useful techniques for measuring majority carrier type, majority dopant ionization energies and majority and minority dopant concentrations. If a resistivity measurement is also performed, the mobility can be determined as well.

To characterize boron implanted layers, boron was implanted in a flat profile pattern as for the BIB detectors, but at lower doses, so that the material does not exhibit hopping conduction. Hopping conduction would prevent observation of the freeze-out of carriers which contains information about ionization energies and minority concentrations. Boron was implanted into a high purity n-type wafer, so the p-type layer will be electrically isolated from the n-type substrate. The donor concentration of the substrate was known for this simple test structure. The wafer was then masked with a piece of silicon and the corners of the sample were implanted to form doped contacts. Samples can be annealed in standard furnaces or in the rapid thermal annealer (RTA). It is extremely important to etch the sides of this structure before doing Hall effect, because the sides have been implanted with stray ions. At low temperatures, the sides provide parallel conduction paths for such a thin implanted layer. The implanted layer on the front surface can be protected during etching with special tape or picene wax. The sides were etched in a 4:1 HNO_3:HF mixture and quenched with methanol. The sample was cleaned with solvents and placed in 5% HF to remove any oxide before attaching wires with pure indium that was pressed into the surface.

Hall effect measurements require a current source, a volt meter, and an electromagnet. The Hall effect measurement system is automated by an IBM 286

computer. Samples are mounted on a cold finger in a Lakeshore CT-210 continuous flow liquid helium cryostat which allows cooling down to approximately 4.5 K. Samples were prepared using the van der Pauw configuration (van der Pauw 1958) and measured in a 3000 Gauss magnetic field.

Figure 2.4 shows the hole freeze-out from 300K to 5K. The two Ge samples both received boron implants with doses of $1x10^{10}cm^{-2}$ at 70keV and $3.1x10^{10}cm^{-2}$ at 200keV. Annealing was performed in an RTA at 600°C for 15 to 20 seconds. We first concentrate on sample 806-10.8. The hole freeze-out between 100K and 30K is due to copper acceptors. The freeze-out slope corresponds to the first ionization of $Cu^{o/-}$ with energy 44meV. The second freeze-out starts at 20K and continues down to 10K. The slope is

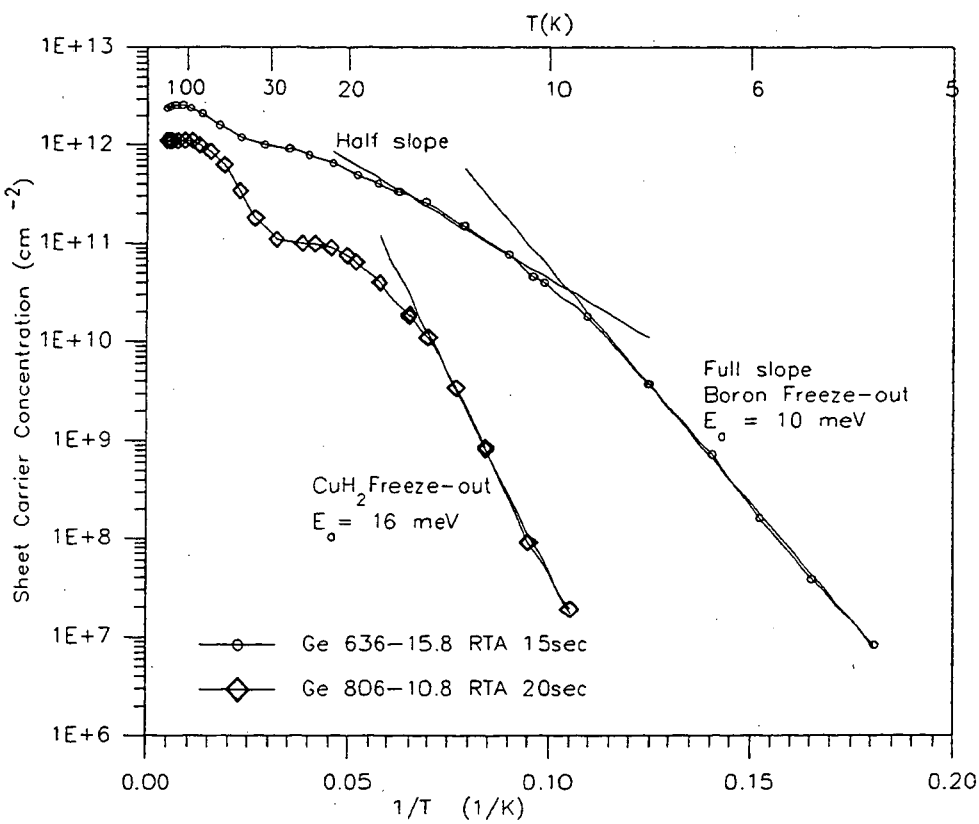

Fig. 2.4. Variable temperature Hall effect of two B Implanted p-type Ge layers

16 meV and corresponds very closely to the ionization of CuH_2, which was also later identified by PTIS. We now concentrate on sample 636-15.8. This sample shows hole freeze-out in three stages. The hole freeze-out between 100K and 30K is again observed. The amount of acceptors that freeze-out in this range is small, and the resulting slope is far too short to allow determination of the impurity's ionization energy. This hole freeze-out is attributed to copper, because the hole freeze-out is in the same temperature range as sample 806-10.8. The second stage of freeze-out is extremely small and it can be inferred that in this range, some concentration of CuH_2 acceptors freeze-out also by comparison to sample 808-10.8. The last hole freeze-out from 10K to 5.5K corresponds approximately to the ionization energy for boron.

It is clear that both samples exhibit a large copper concentration in the implanted region after annealing in the RTA. The difference in the value of the sheet concentration at 100K between the two samples can be explained by different substrate thicknesses. This infers that the substrate has turned from n-type to p-type, because of the activation or introduction of Cu. The type change made it difficult to separate the boron activation from the substrate effects for sample 636-15.8. The Hall measurement shows that Cu was quenched into the Ge substrate at a concentration of $1x10^{13}$ cm^{-3}.

In the VTHE freeze-out curve, the minority concentration can be determined at the transition point of half slope $-E_a/2k$ to full slope $-E_a/k$. To determine the minority concentration, the half-slope of ionization energy is fit to the data. Sample 636-15.8 does not have a distinct plateau due to the boron, because of the Cu and CuH_2 presence. The transition point gives a donor compensation of 4 to 10% of the boron concentration.

2.3.3 PhotoThermal Ionization Spectroscopy (PTIS)

The lack of boron and the presence of another semi-shallow impurity in sample 806-10.8 prompted the study of this sample with PTIS. PTIS is a two step process. Carriers (holes) bound in the ground state of the impurity are excited by a photon up into the bound excited states of the impurity. The second process is the excitation of the carrier into the (valence) band by a phonon. The photoexcitation is measured with Fourier transform infrared spectroscopy (Bell 1972). A Michelson interferometer is used with a chopped IR mercury arc lamp, to be discussed in more detail later. IR photons travel through polished and evacuated brass light pipes to the sample. The ac signal is measured with a lock-in amplifier. This method measures only acceptors in p-type crystals, until dc band-edge light is shown onto the crystal (Lifshits, et al. 1968). Band edge light causes a population of minority carriers to be produced which are trapped by minority impurities. These impurities then generate free minority carriers when they absorb photons and phonons of appropriate energies. The minority carriers decrease the conductivity by recombining with majority carriers in the sample creating negative peaks in the photoconductivity spectra.

Figure 2.5 shows the PTIS spectra for sample 806-10.8. The sample was held at 7K in a glass liquid helium dewar. A 1/2 mil beam splitter was used in the interferometer for an optimum spectral range of 0 to 250 cm^{-1}. The peaks associated with the CuH_2 acceptors appear strongly in the spectrum. It is also apparent in the spectra, that aluminum is a residual impurity in the substrate. The boron in the implanted layer is heavily compensated, because the D and C lines of boron do not appear until band gap

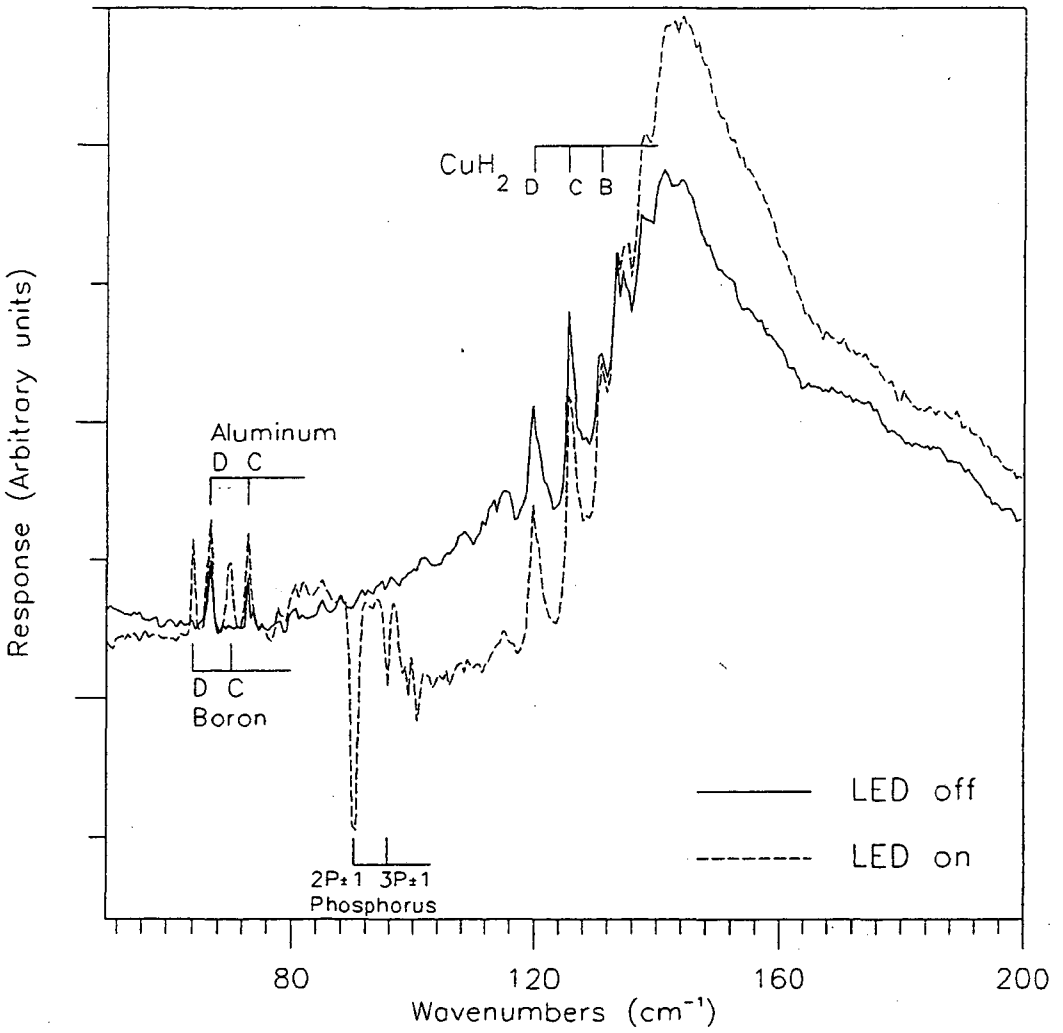

Fig. 2.5. PTIS of boron implanted and annealed Ge 806-10.8

light is shown on the sample, filling the compensated acceptors with holes. The aluminum and boron have similar peak heights because they have similar sheet concentrations. The boron is only near the surface in a thin 0.5 μm implanted layer while the aluminum is through out the substrate. The phosphorus donors in the substrate also appear in the spectrum with band edge light.

2.3.4 Activation of the Ion Implanted Layers

To achieve a fully operational BIB detector, the boron implant must have the highest activation possible to produce banding of the boron acceptors. Ion implantation never leads full electrical activation of the dopant species, because radiation damage may hinder some of the impurities from reaching substitutional sites (Ryssel and Ruge 1986). Boron was implanted into crystal 730-11.0 which had a net acceptor concentration of $\sim 10^{11}$ cm^{-3}. The same energy and range of doses for a BIB detector with a target boron concentration of $3x10^{16}$ cm^{-3} was used. The series was $2.0x10^{11}$ cm^{-2} at 33keV, $5.5x10^{11}cm^{-2}$ at 80keV, $9.5x10^{11}cm^{-2}$ at 200keV, and $1.8x10^{12}cm^{-2}$ at 400keV. The wafer was diced, annealed in Ar, and measured with Hall effect at 77K in a 100 Gauss magnetic field. The results are shown in figure 2.6. The sample with the lower dose of boron was fully annealed at 2 hours at 450°C and reached 65% activation. The sample with the higher dose does not reach its maximum activation of 53% until after 4 hours of annealing at 450°C.

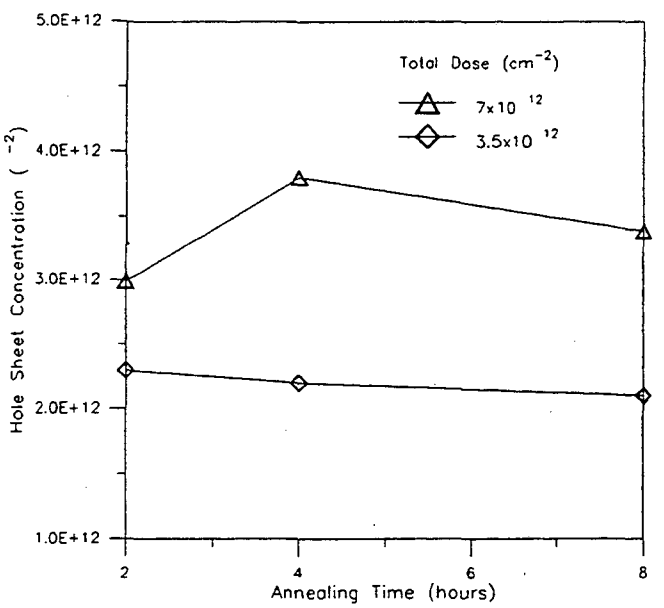

Fig. 2.6 Activation of Boron implanted into Ge and annealed at 450°C.

2.3.5 Deep Level Transient Spectroscopy (DLTS)

A donor concentration of 4 to 10% of the boron concentration was observed with variable temperature Hall effect in the implanted layers. These donors may have levels deep within the gap. The intention was to search for any donor levels and to identify the donor species. If such a donor can be identified, it may be possible to eliminate them and to minimize their effect.

To characterize a material with Deep Level Transient Spectroscopy (DLTS) (Lang 1974), a p-n junction has to be used. When a p-n junction is formed, the potential difference between the p-side and n-side causes a flow of free carriers to equalize the difference. The p-side at the junction becomes depleted of holes and ionized acceptors N_A^- will be left. The n-side at the junction edge become depleted of electrons and ionized donors, N_D^+, will be left. The fixed space charge, N_A^- and N_D^+ created near the junction creates a potential that prevents further diffusion of carriers. By applying an external bias, the diffusion potential can be altered to increase the depletion width (reverse bias) or decrease the depletion width (forward bias). The ability to control the depletion width of a semiconductor p-n junction is used in DLTS.

To fabricate abrupt p-n junctions for DLTS, ion implantation is used. An abrupt ion implanted p^+n junction consists of a heavily doped p^+ layer and a lightly doped n-substrate. Abrupt p-n junctions are used, because the DLTS signal comes from the lightly doped side where the depletion is many times larger. Structures are composed of a rectifying p^+ contact on n-type material with an ohmic n^+ contact on the back. For p-type material, the n^+ contact is rectifying and the p^+ contact is ohmic. The rectifying contact

has a depletion region associated with it that will be probed with DLTS. An example of a diode is displayed in Fig. 2.7.

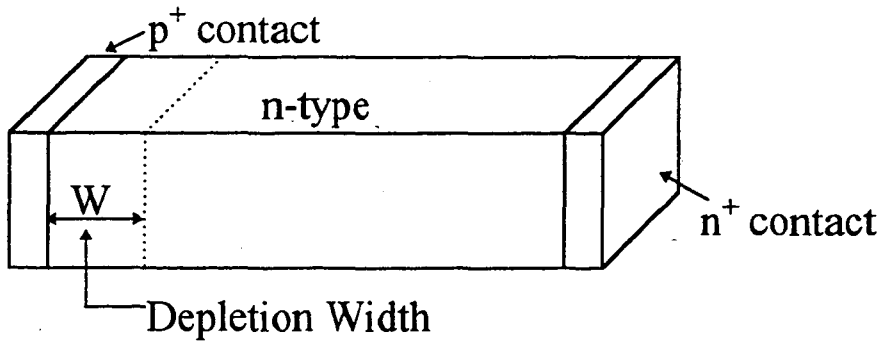

Fig. 2.7 Schematic of p^+nn^+ diode

DLTS is the most sensitive technique for measuring deep levels also referred to as traps in semiconductors. The technique relies on the strong temperature dependence of the carrier emission rate from a deep level. Deep traps are periodically filled by a bias reducing pulse on a reverse biased p-n diode.

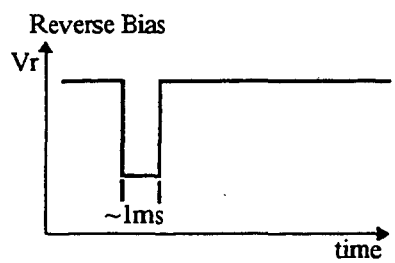

Fig. 2.7. Reduction Pulse in Reverse Bias Voltage for DLTS

During the bias reduction pulse, free carriers rush into the region to compensate precisely the net dopant space charge. Immediately after the reduction pulse, charges compensating shallow levels will be depleted. Depending on temperature, the majority type deep levels hold onto the carriers, and thus the lower concentration of ionized charge in the depletion region leads for a wider depletion region and a correspondingly smaller capacitance. As the carriers are emitted from the deep levels, the capacitance will rise back to its steady

state value. The emission rate of the deep traps can be determined by observing the change in capacitance as the carriers are emitted from deep states, shown in Fig. 2.8(a).

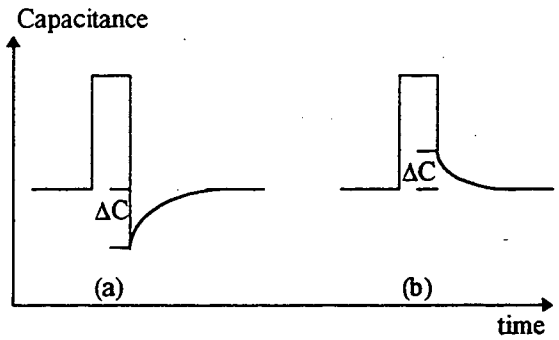

Fig. 2.8 (a) Majority Trap Transient, (b) Minority Trap Transient

The emission rate is a strong function of temperature, shown in equation 2.1.

$$e = \frac{1}{\tau} = \sigma v_{th} N_v \exp(\frac{-E_a}{kT}) \qquad [2.1]$$

In the above equation, σ is the capture cross section, N_v is the effective density of states, v_{th} is the thermal velocity, k is Boltzman's constant, and T is absolute temperature. By measuring the emission rate of carriers from a deep level as a function of temperature, the activation energy, E_a, can be determined by using an Arrhenius plot of $\ln(e/T^2)$ vs. 1/T. The activation energy measured is the enthalpy of the trap. To determine the total free energy of the deep level, the entropy can be measured by determining the temperature dependence of the capture cross section, which is usually small and is often ignored during the activation energy determination. The capture cross section is a measure of the ability of the level to capture a free carrier. A study of the capture cross section reveals information about the nature of the level, namely if it is an attractive, neutral or repulsive trap.

The detection limit for this technique is approximately a deep level concentration 10^{-4} to 10^{-6} times the shallow carrier concentration, N_S. The trap concentration, N_t, can be determined for a majority trap in the limit that $\Delta C/C \ll 1$ by measuring ΔC as shown in Fig. 2.8 using equation 2.2.

$$N_t = 2\frac{\Delta C}{C}N_s \qquad [2.2]$$

The shallow concentration can be found from the slope of $1/C^2$ vs. V.

$$\frac{1}{C^2} = \frac{2}{A^2 \varepsilon\varepsilon_o e N_A}(V_a + V_{bi}) \qquad [2.3]$$

In the above equation, A is the area of the diode, $\varepsilon\varepsilon_o$ is the dielectric constant, N_A is the shallow acceptor concentration, V_a is the applied voltage, and V_{bi} is the built-in voltage of the diode.

Both majority and minority traps can be characterized with DLTS. If the p-n junction is forward biased during the reduction pulse, minority carriers will be present in the depletion region and will fill the minority traps. Both majority and minority carriers are emitted after the bias is returned to the original voltage. Since minority deep levels have the opposite charge than majority deep levels, the capacitance is higher after the reduction pulse as shown in Fig. 2.8(b). Determining the concentration of minority traps is extremely difficult because the free minority carrier concentration during injection is unknown. This technique of characterizing minority traps is called injection DLTS or minority DLTS.

Deep levels with different energies will have different emission rates. In measuring the temperature dependence of the emission rates, deep levels will appear in different parts

of the temperature spectrum. If two deep levels have similar energies, the two signatures will be difficult to separate.

Accurately measuring time constants of exponential signals from emitting traps poses a challenge. The correlation method has been shown to be the most sensitive for analyzing exponential transient signals (Miller, et al. 1975). This method works by electronically multiplying the exponential capacitance signal, $e_1(t)$, with a set exponential weighing function, w(t). This product is then integrated, shown in equation 2.4. The integrated signal, $e_o(T_m)$, reaches a maximum when the time constant of the signal is equal to the set time constant.

$$e_o(T_m) = \int_0^{Tm} e_1(t)w(t)dt \qquad [2.4]$$

Signals with larger or smaller time constants produce a reduced output shown in Fig. 2.9.

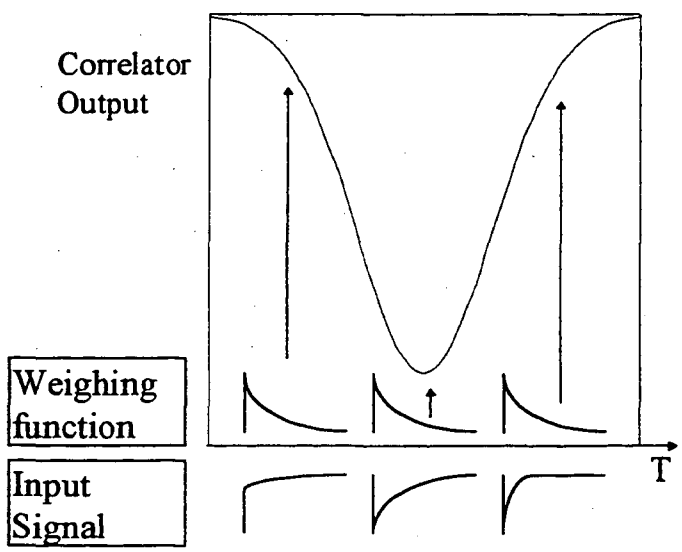

Fig. 2.9 Schematic of correlator output of a deep level

Miller described the output line shape, shown in equation 2.5, in terms of α, which is a dimentionless quantity of $\alpha = T_s/T_m$, which is shown here for completeness. T_s is the time

constant of the signal and T_m is the integration time, which is usually set to $T_m=4T_R$. T_R is the reference time constant of the weighing function. The holdtime is the time after the start of the reduction pulse at which integration begins, so that the reduction pulse is not integrated over.

$$A(\alpha) = \frac{\alpha + \exp(-(\alpha+1)/\alpha)}{\alpha+1} - \exp(-1/\alpha) \qquad [2.5]$$

2.3.6 DLTS of Boron Implanted into p-type Ge

Boron implanted layers in Ge have been studied with DLTS and 3 majority hole traps have been identified (Jones 1985). Their activation energies were E_v+0.17eV, E_v+0.23eV, and E_v+0.37eV. A further study was undertaken to identify a donor responsible for compensating these implanted layers. This donor could be identified by performing injection DLTS and identifying an electron trap.

DLTS studies were done on implanted layers after low temperature anneals. The spectrum changes drastically with annealing. Many different annealing parameters were used in case the donor was visible during the change. Minority donor signals could easily be overwhelmed by the majority acceptor signals.

Diodes for characterization of an implanted layer were fabricated and annealed. Boron was implanted for the ohmic contact on p-type Ge and phosphorus for the rectifying contact. The boron was implanted at 33keV with $1\times10^{14}cm^{-2}$ and 50keV with $2\times10^{14}cm^{-2}$ at room temperature leading to a 0.3 μm layer. The phosphorus was implanted at 103K using liquid nitrogen cooling to form an amorphous layer 0.15 μm thick. This was done because activation of phosphorus is improved by using solid phase epitaxy (SPE) (Csepregi, et al. 1977). of the amorphous implanted layer and was shown to be a

more blocking contact for radiation detectors (Pehl 1985). Phosphorus was implanted at 40keV with $2x10^{14}cm^{-2}$ and 100keV with $4x10^{14}cm^{-2}$. The structure was annealed from 50°C to 330°C in 15 hours. See Appendix C for the phosphorus contact's sheet resistivity and concentration as a function of temperature.

After the diodes were fabricated and annealed, boron was implanted at high energies through the already annealed phosphorus implanted contact into the depletion region of the diode. The boron for characterization was implanted with a dose of $3x10^{10}cm^{-2}$ at 400keV, $1.8x10^{10}$ cm^{-2} at 200keV, and $0.9x10^{10}$ cm^{-2} at 90keV.

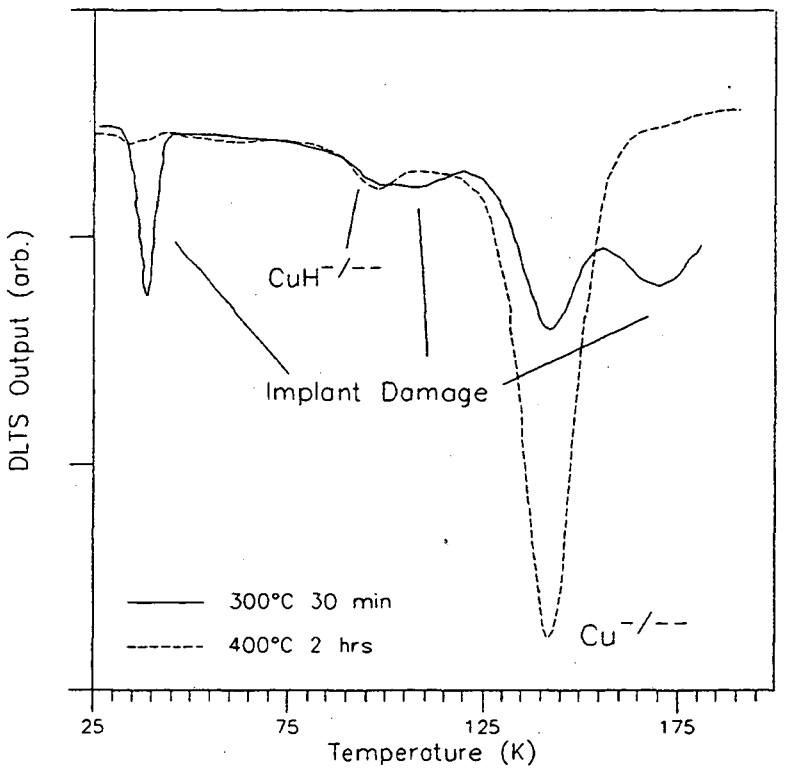

Fig. 2.10 DLTS of Boron Implanted into p-Ge

At zero bias, the whole boron implanted layer to be characterized is self depleted by the diffusion potential of the n^+p junction. The diode must be put into forward injection during DLTS to probe the implanted region. Figure 2.10 shows typical spectra from two annealed samples measured at τ=12 ms.

Implantation damage hole traps dominate the DLTS spectrum after low temperature annealing. At higher annealing temperature and longer times, the defects anneal away and Cu peaks dominate the spectrum. Any electron trap's signature would be overwhelmed by the large hole trap signals and the deep donors would not be observed. Many samples were annealed to try to observe an electron trap in the transition range where radiation damage traps have annealed away and the Cu trap concentration is increasing. After the study of 10 samples using different annealing schedules, no minority peaks were found.

2.3.7 DLTS of Boron Implanted into n-type Ge

Since no donor defect could be found for boron implants in p-type Ge, boron was implanted into n-type Ge below the donor concentration, so that the region remained n-type after implantation. Observing a donor in n-type material is much easier than in p-type crystals. The crystal, S-18, was antimony doped to a concentration of approximately 10^{15} cm^{-3}. Boron was implanted through an annealed boron contact into the n-type bulk resulting in the doping profile shown in Fig. 2.11.

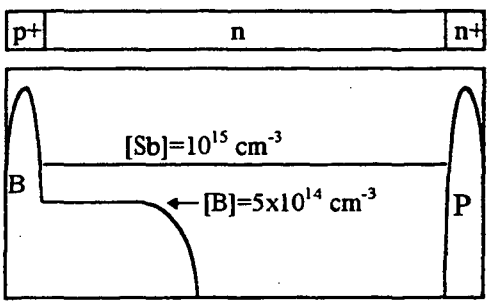

Figure 2.11 Diode structure for DLTS of boron implant in n-Ge.

Under forward injection (2.0V bias, 2.1V pulse), the boron implanted region is sampled with DLTS. The pulse width of 0.8 ms and a holdtime of 1.8 ms were used. A trap with a

maximum emission at 190 K at a time constant of 12 ms appeared. The activation energy of this trap is E_c-335 meV. This level is not present in the unimplanted portion of the sample, which was probed under majority conditions (2.0V bias, 1.0V pulse).

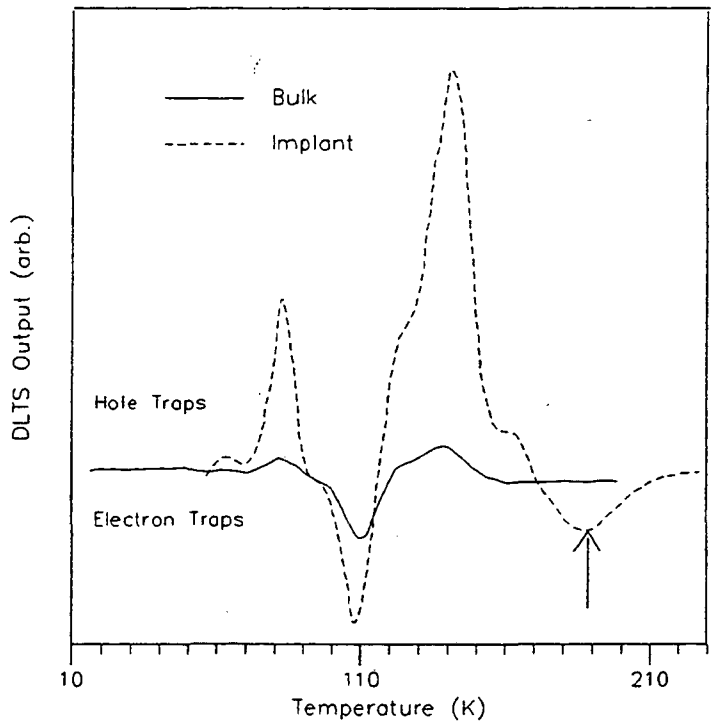

Fig. 2.12 DLTS of Boron Implant in n-Ge.

The two spectra are shown in figure 2.12. The 0.335eV electron trap is assigned to a deep level resulting from the boron implantation. The variation of the capture cross section with temperature is displayed in Table 2.1.

Temperature	138 K	144 K	157 K	164 K
σ (cm^2)	1.8×10^{-17}	5.9×10^{-18}	5.7×10^{-18}	5.8×10^{-18}

Table 2.1 Capture Cross Section of 0.335eV

The low values and weak temperature dependence of the capture cross section suggests that the electron trap's charge state is neutral, although it could be a weakly

attractive donor. This data does not allow us to precisely identify the deep level as a donor.

The speculation for the electron trap to be a donor is based on the following arguments. In n-type Ge with the Fermi level near the conduction band, an acceptor must be negatively charged. During the forward injection pulse, the acceptor could trap a hole to become neutral, but the release of that hole would produce a minority signal in DLTS. We observe a majority signal from the release of an electron to the conduction band. We assign the E_c-0.335eV level to a donor associated with the boron implant. Annealing studies were not performed on this donor, because of the limited quantity of antimony doped germanium.

3. Characterization Results for BIB Detectors

3.1 Dark Current-Voltage and Spectral Response Techniques

The spectral response of an IR detector shows in what range the detector can be optimally used. The dark current versus bias voltage measurement (I-V) is a gauge of the impedance of the device and the noise that is associated with current flowing in the absence of external light. Spectral response and dark current-voltage measurements are made with a detector mounted in an Infrared Labs H3 dewar on a liquid helium cold stage. The temperature of the detector can be dropped from 4.2 K to 1.3 K by pumping on the liquid He bath, because reducing the vapor pressure lowers the boiling point of the liquid helium. It is important to test these detectors at the low temperatures, because the detector's impedance rises with decreasing temperature and dark currents decrease. The dopant impurities are "frozen-out" at these low temperatures increasing the impedance. The short wavenumber response is also improved, because more neutral impurities will be available for photoionization.

An I-V measurement is taken by applying a voltage to the detector and measuring the voltage over a feedback resistor of approximately 10^{10} Ω. The range of the detector circuit is between 10^{-9} and 10^{-15} A with the 10^{10} Ω feedback resistor. A schematic of the transimpedance amplifier circuit with a matching pair of cold JFETs in Fig. 3.1. A shutter in the IR Labs dewar allows the device to be shielded from almost all external radiation. With the shutter closed, the detector is surrounded only by the liquid helium blackbody radiation.

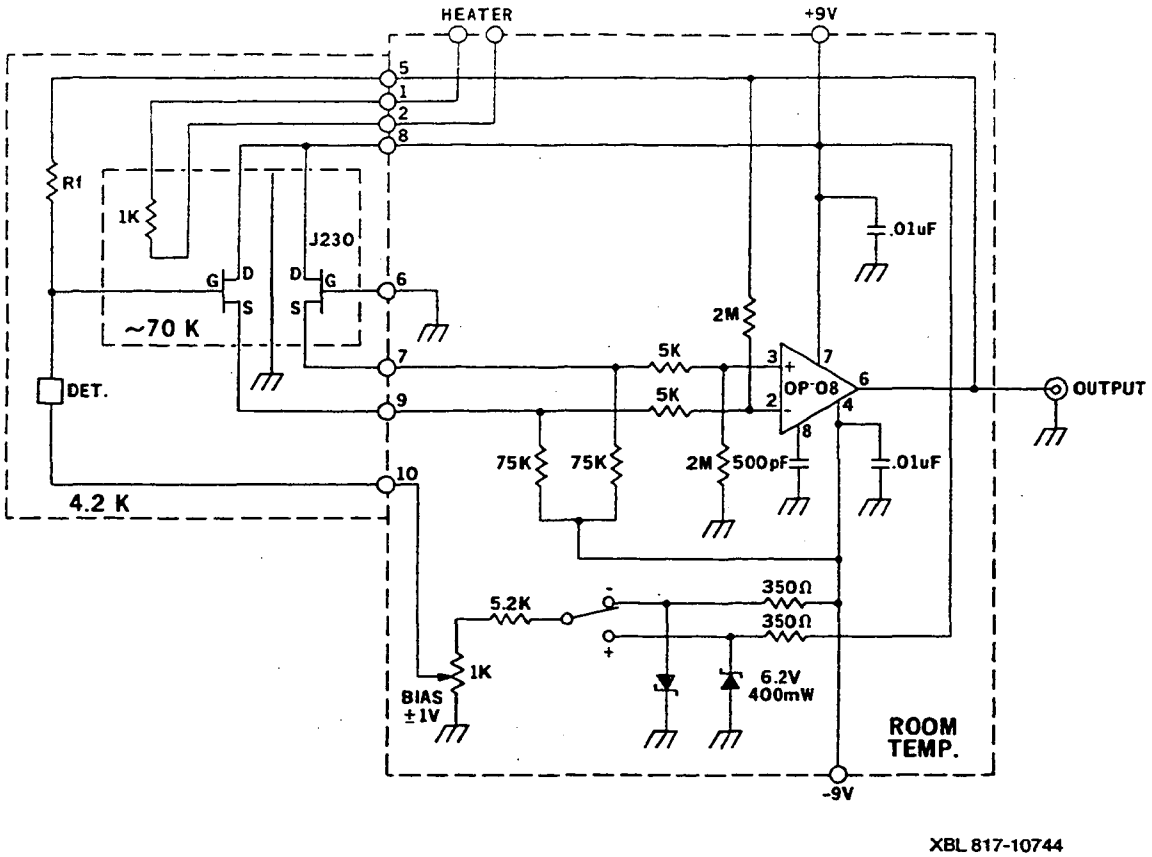

Fig. 3.1 Transimpedance Amplifier Schematic.

Spectral response of a detector is measured by using a far infrared Fourier transform spectrometer. A schematic of the interferometer is shown in Fig. 3.2. The spectrometer has 4 different mirrors, a parabolic mirror M_p, a fixed mirror M_f, a movable mirror M_m and a off-axis paraboloid M_{op}. The light from the source S is parallel after reflection off the parabolic mirror. The light travels through the beam splitter BS and is split into two beams. One beam is reflected by a fixed mirror and the other by the movable mirror. The two beams are sent back to the BS where they recombine. The movable mirror changes the path length of one beam. The difference in path length of the two beams causes some wavelengths to interfere constructively and some destructively.

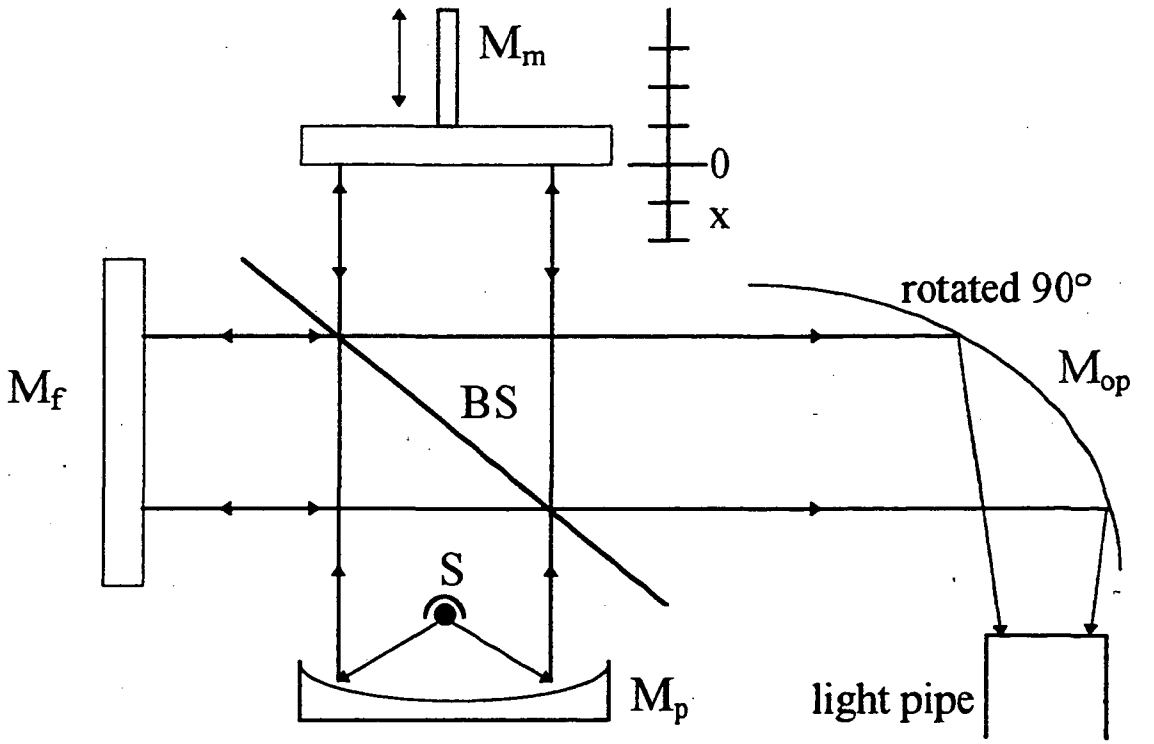

Fig. 3.2 Schematic of Fourier Transform Spectrometer

The changing interference produces a cosine response modulation in the intensity of the exit beam called an interferogram. A Fourier transformation of the interferogram is numerically performed and yields the spectrum.

The far infrared Fourier transform spectrometer operates from 0 to 500 cm^{-1} with a 1/4 mil mylar beam splitter. The instrument response is shown up to 250 cm^{-1} in Fig. 3.3 measured at 14.3 Hz chopping frequency with a golay cell. The instrument response at smaller wavenumbers can be improved by using a thicker beam splitter. The 1/2 mil beam splitter has about half the efficiency at 50 cm^{-1} compared to the 1 mil beam splitter. By using a 1 mil thick mylar beam splitter, the instrument gain can be maximized at low wavenumbers around 50 cm^{-1}, which is the region of interest for a working Ge:B BIB detector.

The interferometer is evacuated to 0.1 militorr in order to eliminate water vapor and CO_2 absorption. The far IR source is a mercury arc lamp with a ~50% of the IR output from the arc and the remaining 50% from the hot quartz envelope. Outside the interferometer the light travels out through polished brass light pipes that are evacuated to 30 militorr to remove interference from absorption. The light enters the dewar

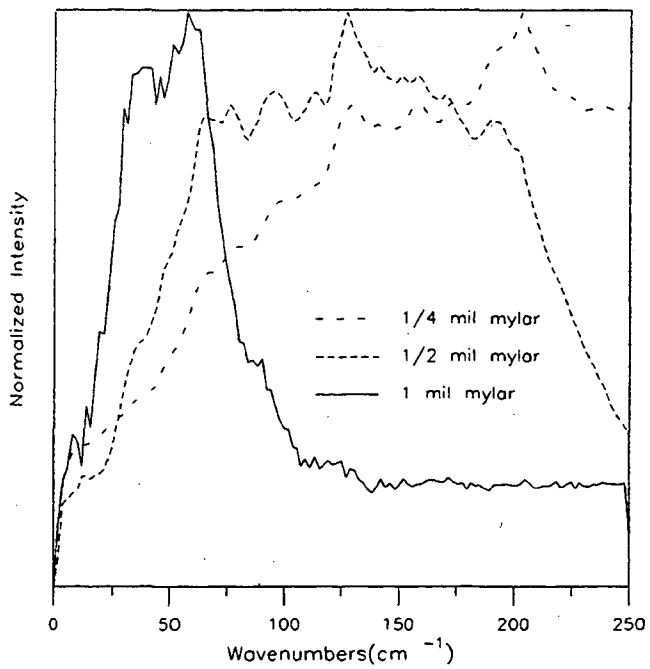

Fig. 3.3 Instrument Response of beam splitters in Far Infrared Fourier Transform Spectrometer

through a polyethylene window, travels through the liquid nitrogen cooled aperture and the liquid helium cooled aperture. An 8 mil thick black polyethylene filter was placed in the light path to eliminate above band gap light and transmit the far IR light. The detector response was measured using the transimpedance amplifier in Fig. 3.1.

3.2 Bulk Boron Implanted Detectors

3.2.1 Results for High Energy Boron Implanted BIB Detectors

BIB detectors fabricated with Wu's design were tested. These detector were investigated, because the planar ion implanted detector had not yet been produced. Dr. G.

Pensl performed boron implants up to 2 MeV with a special implanter at the Universität Erlangen-Nürnberg. The high energy implants allowed a greater absorption to be achieved, because boron ions can reach a depth of 3.1 μm. The implantation series used is given in Table 3.1.

Energy (keV)	33	150	220	350	550	770	1020	1300	1600	2000
Dose ($x10^{11}cm^{-2}$)	5000	9	9	9	9	9	9	9	9	20

Table 3.1. Energy & Dose: Implant Series for High Energy BIB Detector

In Fig. 3.4, curves obtained at different temperatures are shown. The curves are very asymmetric, which is a characteristic of a properly working BIB detector. In reverse bias the blocking layer prevents dark currents from flowing, but it forward bias, carriers will start to stream through the device. The measurement at 1.3K exhibits the lowest dark currents in the reverse bias direction.

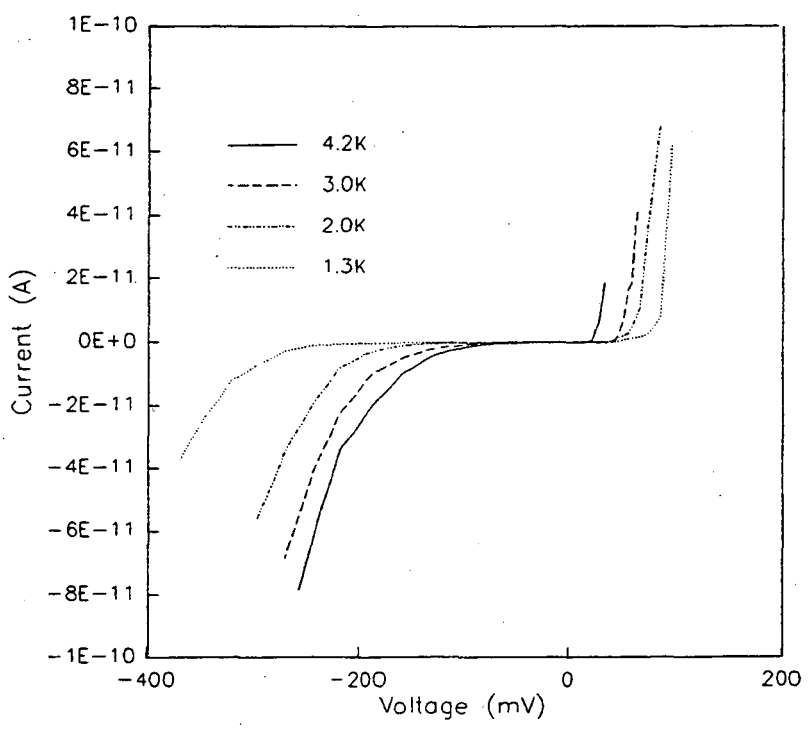

Figure 3.4 I/V Curve of High Energy Boron Implanted BIB Detector Ge730-8.2

The 730-8.2 BIB detector spectral response is displayed in Fig. 3.5. The boron implanted BIB detector in Fig. 3.5 had a blocking layer thickness of 50 μm and was biased at -200mV. The chopping frequency was 23.3 Hz and the temperature was 1.3K. The detector has a response due to CuH_2 between 150 cm^{-1} and 250 cm^{-1}. At 250 cm^{-1}, the 1/2 mil beam splitter efficiency goes to zero, but rises at higher wavenumbers. The detector also has a response due to the first ionization of Cu between 300 cm^{-1} and 450 cm^{-1}. At 340 cm^{-1}, the dip in the Cu response is attributed to multi-phonon absorptions. The region, around 80 to 120 cm^{-1}, where the detector should have a large boron response surprisingly shows no response. This is currently not understood.

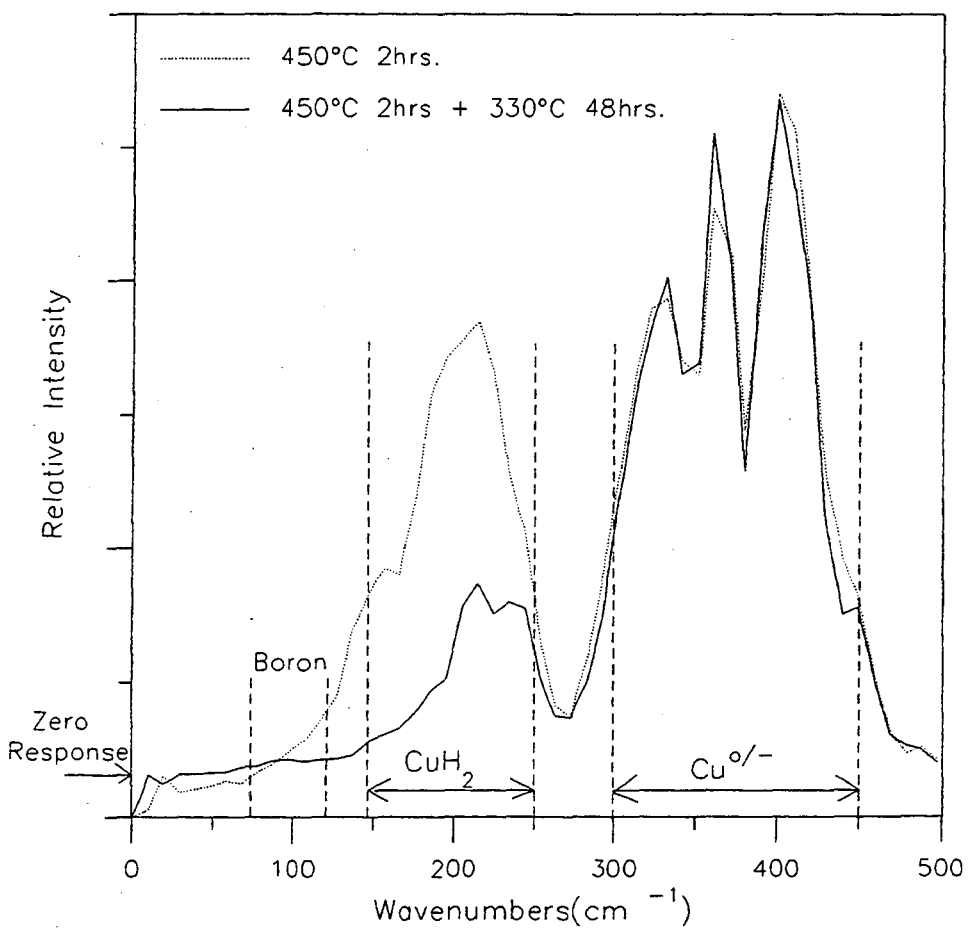

Fig. 3.5 Spectral response of High Energy Boron Implanted BIB Detector Ge 730-8.2

Because this high energy boron implanted BIB detector showed such large CuH_2 and Cu responses after annealing at 450°C for 2 hours, further annealing was performed to observe any change in the Cu concentration. Cu can be precipitated out of the material by annealing at low temperatures. A decrease in the concentration of CuH_2 relative to the $Cu^{0/+}$ concentration was observed after annealing at 330°C for 48 hours. The $Cu^{0/+}$ photoconductive peak was normalized for comparison.

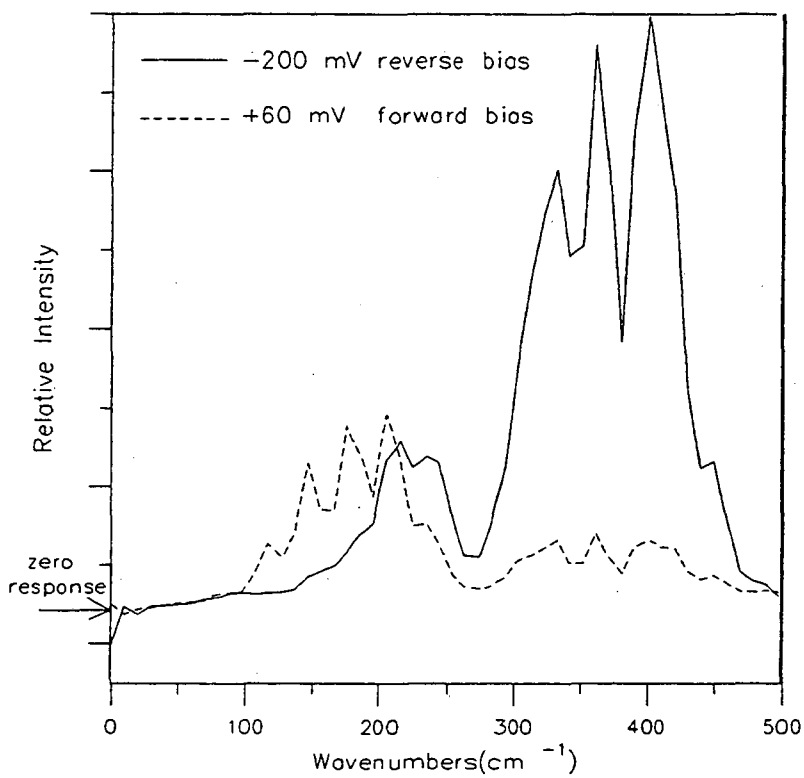

Fig. 3.6 Bias dependence of spectral response of high energy boron implanted BIB detector Ge 730-8.2

The bias dependence of a high energy boron implanted BIB detector is shown in Figure 3.6. This detector was measured in the 0 to 500 cm^{-1} range, because it has information about the processes that occur in the material depending on the position in the device. The detector does not exhibit shallow dopant response at 100 cm^{-1} under normal operating conditions of reverse bias, but does in forward bias. Under reverse bias, the

BIB detector depletes from the interface between the blocking layer and IR active layer, where the implantation energies are the highest. It is propose that the boron implanted at higher energies is less activated than the boron near the surface that was implanted with lower energies. The lack of activation could be a passivation or compensation issue, but this is not known at his point in time. The DLTS work in n-type Ge suggests that a donor compensates the boron. At this interface, the IR active layer is not depleting and photoionization events will be minimal. Under forward bias, the implanted layer depletes from the interface between the contact and the IR active layer, where the absolute donor concentration may be lower. If the donors are implantation induced defects, the lower damage may reduce its concentration. This hypothesis explains the boron response during forward bias and the absence of boron response under reverse bias in Fig. 3.6.

Donor defect formation may be associated also with impurities in the Ge crystals, so a low oxygen germanium crystal was used for the high energy implanted BIB detector. A comparison was made with crystal 564 because it was grown from a graphite susceptor and should have less oxygen compared to the SiO_2 crucible grown crystals. Oxygen in silicon has been shown to form donors when thermally treated (Wagner, et al. 1984). It is possible that oxygen in the germanium was limiting the device performance of the ion implanted BIB detectors because it may have formed thermal donors.

The low-oxygen detector was annealed at 450°C for 2 hours. This detector was measured with a 1/2 mil beam splitter. The measurement was performed at 23.0 Hz, 1.3K, and a bias of -64 mV. This detector also shows a strong Cu response. Unlike the 730-8.1 boron implanted BIB detectors, this boron implanted BIB detector shows a boron

dopant response as shown in Fig. 3.7. A second response was taken with a low pass LiF filter below 200 cm^{-1}. This allowed better characterization of the shallow boron response, but it appears that the 564-8.1 boron implanted BIB detector still did not exhibit extended response.

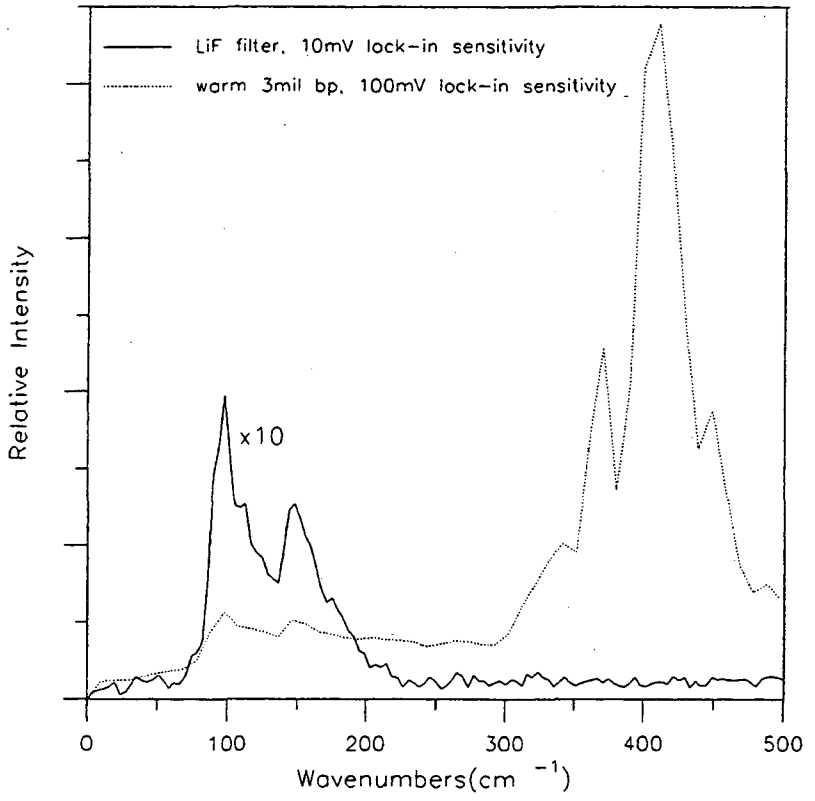

Fig. 3.7 Spectral response of high energy boron implanted BIB detector Ge 564-3.1

3.2.2 Results for Low Energy Boron Implanted BIB Detectors

With the Varian implanter at Lawrence Berkeley Laboratory, boron can be implanted at energies up to 400 keV by using doubly charged ions. The boron series implanted at low energies (LE) to form a BIB detector was 3.6×10^{12} cm^{-2} at 400keV, 1.9×10^{12} cm^{-2} at 200keV, 1.1×10^{12} cm^{-2} at 80keV, and the contact dose was 2×10^{13} cm^{-2} at 33keV. The desired doping for this detector for the IR active layer was 6×10^{16} cm^{-3} to a

depth of 1 μm, which is double the dose used for previous high energy boron implanted detectors. This detector shows a boron response at 80 cm^{-1}, which is at slightly lower energies than the known ground state of boron at 87 cm^{-1}, shown in Fig. 3.8 The lower energy response verifies that the boron level is beginning to band, but clearly the response is far from the 50 cm^{-1} wavenumber goal.

I.C. Wu(Wu, et al. 1991) observed that the response of his detectors would shift to lower energies when increasing the reverse bias. It was argued that his detectors were depleting into more heavily banded region at higher biases. Two spectra were taken with this detector, and no shift in response could be observed due to higher bias, shown in Fig. 3.8. We do not understand this discrepancy in the two sets of measurements.

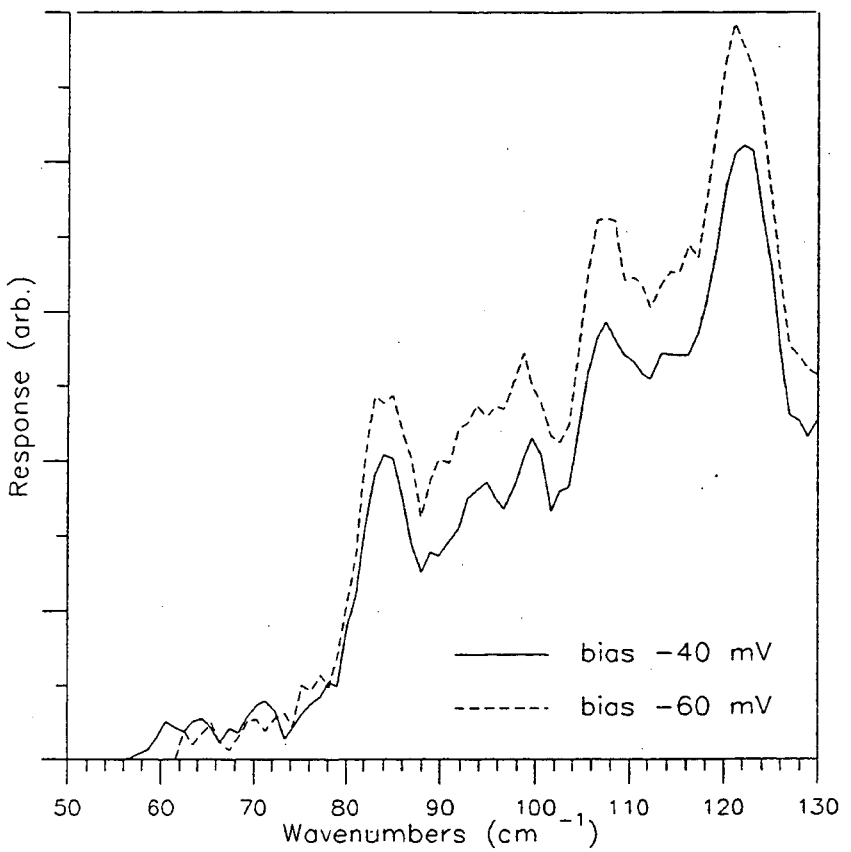

Fig. 3.8 Spectral response of low energy boron implanted BIB detector 730-11.0

3.3 Planar Boron Implanted BIB Detector Results

3.3.1 Asymmetric Devices

BIB detectors have an asymmetric geometry due to the IR active and blocking layers. The planar BIB detectors described in section 2.2 is therefore asymmetric. It is again shown in Fig. 3.9(a). The structure of the asymmetric planar BIB detector causes the depletion to be parallel to the surface in the IR active region.

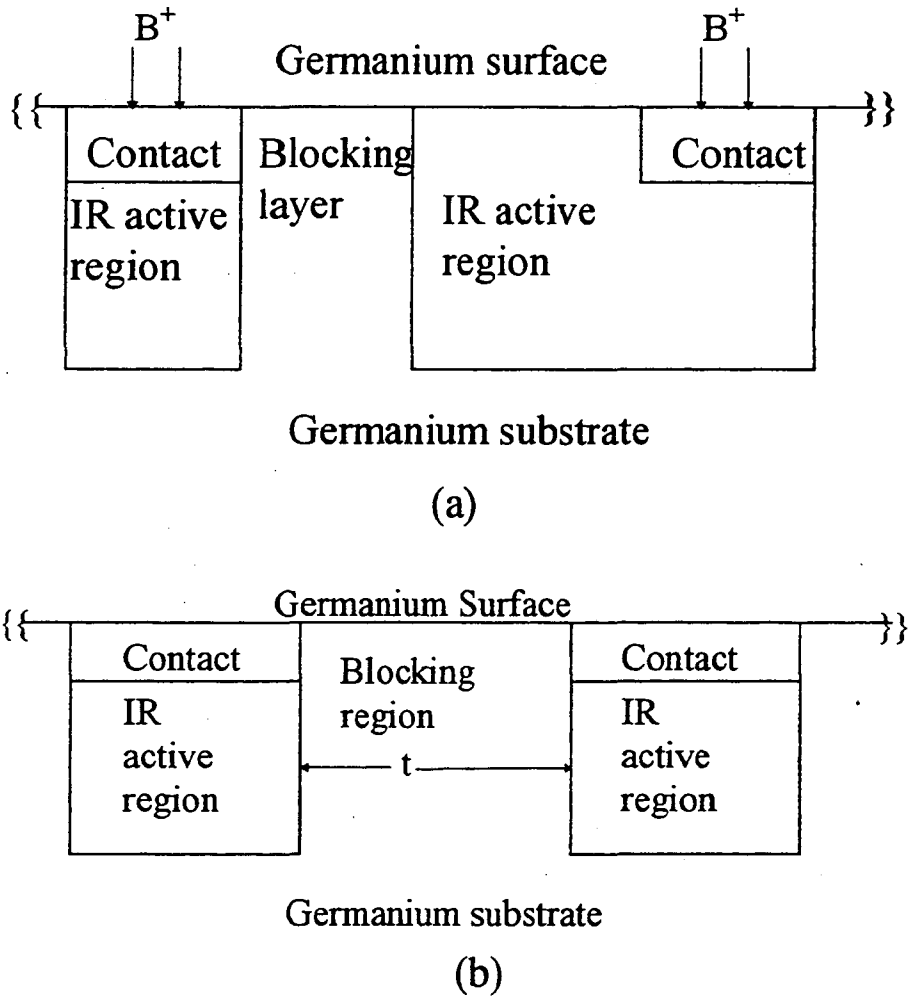

Fig. 3.9 Cross section of (a) Asymmetric (b) Symmetric BIB Detectors

These asymmetric devices have been fabricated, but the misalignment between the contact and IR active region masks has been around 2 to 3 microns, which would prevent the device from performing properly. No spectral response measurements have been made

on these devices. The difficulty in fabricating asymmetric devices necessitated the fabrication of a simpler device. This device geometry turns out to be symmetric and will be referred to as a symmetric planar boron implanted BIB. The implanted IR active region was only directly underneath the contacts, so the geometry is symmetric in the cross sectional view, shown in Fig. 3.9(b). This simplification omits the need for precise alignment between the contact mask and the IR active region mask.

All of the IR active region in the symmetric BIB detector is shadowed by the contacts at the surface. Therefore, the asymmetric BIB should absorb a greater fraction of the incident photons in the signal forming region than the symmetric BIB. Fabrication of another set of asymmetric devices will be attempted because of their potential advantages over the symmetric devices. Alignment procedures have been improved by removing vibrations from a fan in the Kaspar mask aligner.

3.3.2 Symmetric Devices

The symmetric planar ion implanted BIB detector has the IR active layer directly beneath the contacts. Although the contacts are transparent to most of the light, they do absorb about 20% of the photon flux measured in the spectral range 70 to 140 cm^{-1}. The spectral dependence absorption measurement is described in Appendix IV. The advantage of the symmetric ion implanted BIB is that there is no misalignment error between the contacts and the IR active absorbing region.

A symmetric planar boron implanted BIB was fabricated using Ge crystal 639-8.1. Boron was implanted with a target concentration of $3x10^{16}$ cm^{-3} in the IR active region. The planar BIB was annealed at 450°C for 2 hours in N_2+4%H_2 flowing gas to remove

implantation damage. For the response measurements, the chopping frequency was 23.0 Hz, the 1 mil beam splitter was used, and the operating temperature was 1.3 K. The spectral response is shown in Fig. 3.10. The response at high wavenumbers drops off due to the 1 mil beam splitter efficiency, shown in Fig. 3.3.

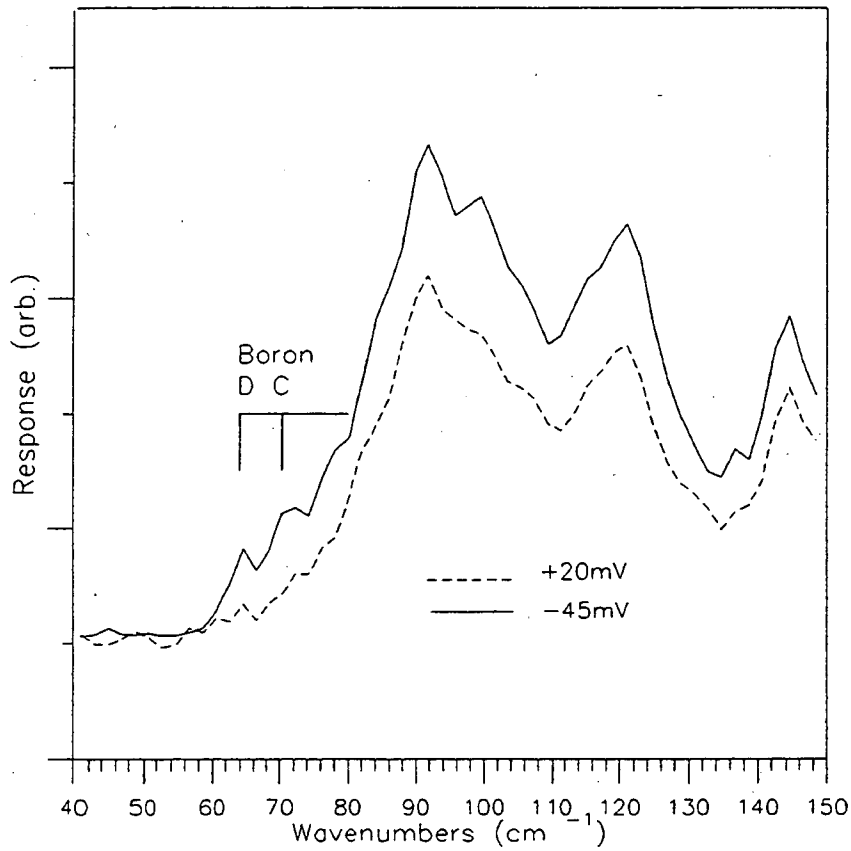

Fig. 3.10 Spectral response of symmetric planar BIB 639-8.1 10 μm blocking layer

The planar BIB detector showed wavenumber response down to 60 cm^{-1}, which is a significant improvement towards to the 50 cm^{-1} goal. The 64 cm^{-1} peak corresponds to the D line of boron. The next higher wavenumber peak seems to be contributed mainly by the C line. The boron level has banded much more than previously observed in other boron implanted BIB detectors.

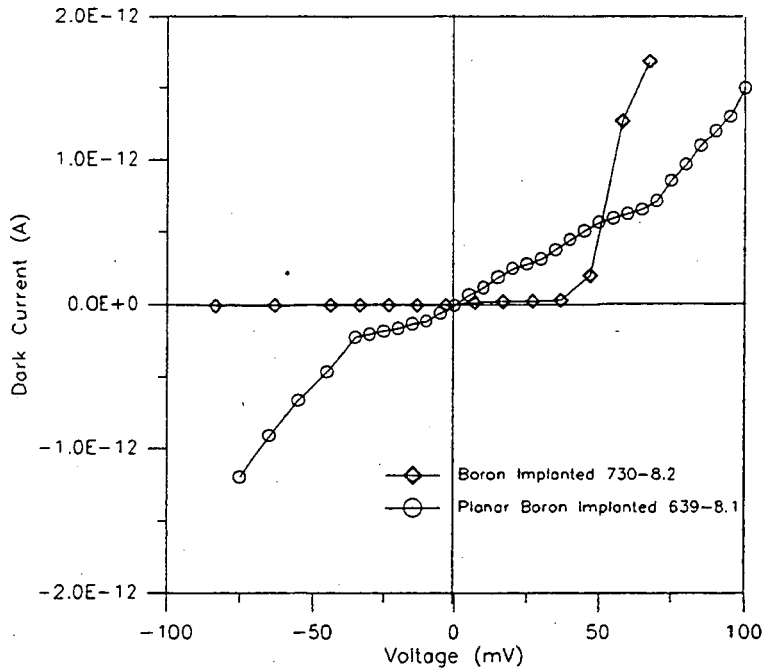

Figure 3.11 Dark I/V of 730-8.2 boron implanted BIB and symmetric planar BIB 639-8.1

The dark I/V was measured at 1.3K, and is shown in Fig. 3.11. The 730-8.2 boron implanted BIB detector had much better dark current than the planar BIB. The dark current results are compatible with the spectral response measurements, i.e., there was no hopping conduction occurring between the boron levels in the 730-8.2 detector, but significant hopping conduction for the planar BIB. Therefore the planar symmetric BIB detector is expected to be "leakier."

4. Discussion

4.1 Small Wavenumber Response

Ge BIB detector response shown in figure 3.8 has promise in the small wavenumber region for low energy implants, because the spectral response begins to increase at a slightly lower energy than the photoconductive onset of boron at low concentrations. This indicates that the boron ground state wavefunctions begin to overlap

and the width of the boron level has increased, decreasing the ionization energy to the valence band. The BIB detector response in figure 3.8 rises strongly at 80 cm^{-1}, which is an improvement from previous detectors.

The planar BIB detector response in figure 3.10 also increases at 80 cm^{-1}, but it also shows response between 60 and 80 cm^{-1}. This increased response is probably due to the decrease in the blocking layer width and therefore greater depletion in the heavily doped region. The symmetric planar BIB had a blocking layer of 10 μm, while the other boron implanted BIB detectors had blocking layers of 50 μm. The spectral response was recorded with an instrument resolution of only 1.9 cm^{-1} to provide the shape of the response. A higher resolution measurement may resolve more features. Increase in the response at 60 cm^{-1} or lower may be improved by two methods. First, by increasing the dose, the response strength of the excited states can be improved. Second, by decreasing the blocking layer width, t, shown in figure 3.9b, from 10 to 5 μm the depletion of this device would improve, as described by equation 1.6.

4.2 Absolute Donor Concentration and Cu Contamination

Limited device performance has been attributed to increased donor concentrations in the IR active layer. Until now, no unusual donors have been identified in p-type Ge, however the detectors shown in figures 3.5, 3.6, and 3.7 show photoresponse due to Cu and CuH_2. Cu must be activated during device fabrication or diffuse in from the surface, because it was not electrically active in the starting material. The concentration of Cu was found to be much higher that of CuH_2 from Hall effect and spectral response measurements. It has been postulated that Cu impurities may form complexes or

compensate as interstitial donors, and that structural defects due to implantation may aid in the creation of these donors. Ion implantation creates collision events which displace atoms from their lattice sites if the energy transferred is greater than the displacement energy. Implanted ions experience a cascade of collisions with the host lattice before the ions stop. These collisions create many defects such as vacancies, interstitials, and complexes.

Many factors can explain the high Cu concentration in these implanted layers. Many Ge crystals contain large concentrations of passivated Cu in the form of CuH_3 after crystal growth (Andreev, et al. 1994). Cu is also found precipitated at dislocations that will become electrically active when the sample is annealed. This provides a large reservoir of Cu for possible future reactions. Cu interstitials diffuse very rapidly in germanium but eventually return to substitutional sites. The substitutional concentration of Cu is higher than its interstitial concentration at elevated concentrations(>450°C), as shown in Fig. 3.12 (Hall and Racette 1964).

A study to attempt to understand all of the interactions of Cu within a Ge crystal is underway. Many impurities such as hydrogen, carbon, and oxygen can interact with Cu. These impurities have approximate concentrations of 10^{14} cm^{-3} in most as-grown Ge crystals. The interaction of these impurities with Cu may form donor complexes raise the absolute donor concentration and lower depletion of the IR active layer. Very little is known about their behavior.

The solubility of Cu_s in Ge shows a strong temperature dependence. This fact has been used in device processing to decrease the electrically active Cu. As the temperature

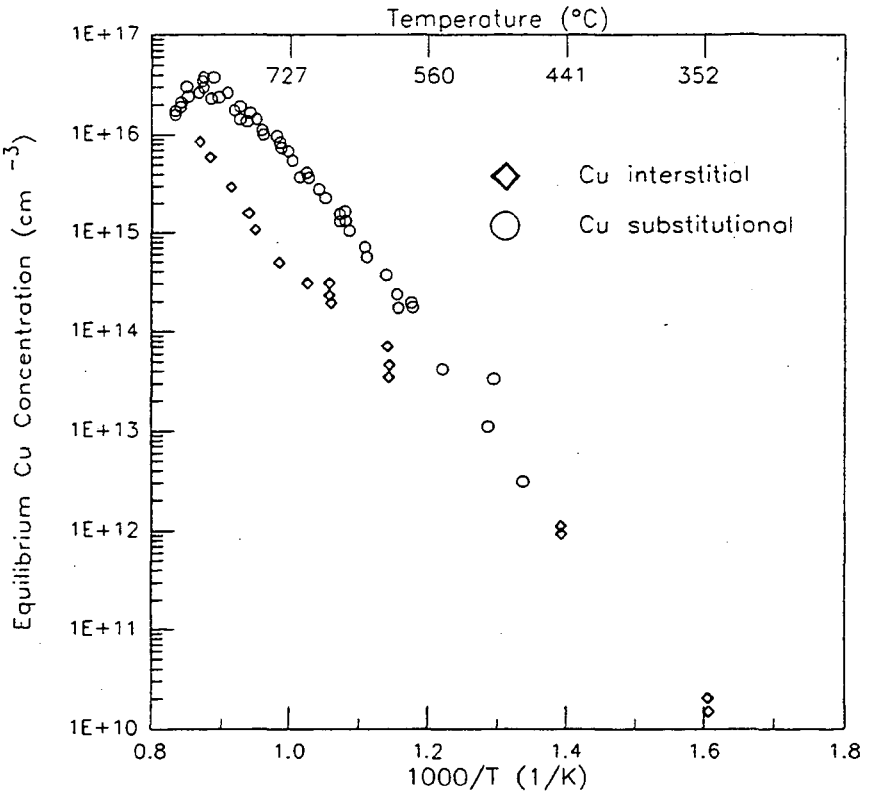

Fig. 3.12 Equilibrium Cu interstitial and substitutional concentrations in p-type Ge.(Hall and Racette 1964)

is lowered, Cu becomes supersaturated in the crystal and will diffuse to sinks. A sink can be a surface, a dislocation, a precipitate, or a region of strain, where the free energy can be lowered. The deliberate removal of unwanted impurities is called gettering. An implanted layer can getter these fast diffusing impurities by providing defects as sinks. During annealing, secondary defects form and trap migrating species. This process may help to form donors and/or complexes in the boron implanted layer. Gettering in silicon has been well studied (Lecrosnier 1983) and is often used as a processing step during device fabrication, while gettering in germanium has not been investigated. Gettering may be a useful method to reduce the Cu concentration.

4.3 Future Studies

Two studies are proposed for the further improvement of boron implanted BIB detectors. The first is to study the doping dependence of the extended wavelength response. The implant dose in the IR active layer should be incrementally increased. The total activated concentration of boron will increase accordingly. The increased acceptor concentration should cause greater banding, which causes absorption at smaller wavenumbers. An absorption experiment should be performed to observe the banding of boron as a function of dose. This increased absorption should improve the spectral response.

Another area for improvement concerns the removal of Cu and other impurities from the Ge crystal by gettering before, during and after detector fabrication. A crystal of 150 μm thick could be purified by a cyclical process of implanting, annealing, and etching. After a couple of cycles, the concentration of fast diffusing species could be diminished if the contamination is only from the crystal. The boron implanted BIB detector now could be fabricated in germanium purified of fast diffusers.

A different approach for gettering Cu is the use of a pure gold layer on the germanium surface as a sink for Cu. Cu has a higher solid solubility in Au that in germanium. Interstitially diffusing Cu should diffuse and accumulate in the gold. W. L. Hansen performed H gettering in a similar manner using gold on the surface (Hansen, et al. 1982). Significant gettering did not occur until 500°C when the gold formed a eutectic liquid with the germanium. In BIB fabrication, the formation of a eutectic liquid would destroy the morphology of the 1 μm boron implanted layer, so gold getting studies would have to be done before the detector fabrication or below the eutectic temperature 362°C.

5. Conclusion

Due to the difficulty of Ge epitaxial growth, boron implanted BIB detectors have been fabricated in germanium and tested. Asymmetric planar BIB detectors were produced, but so far have not worked because of misalignment error of the implantation masks during fabrication. Symmetric planar boron implanted BIB detectors do not need the crucial alignment step during fabrication. These BIB detectors have shown response at 60 cm^{-1}. Future detectors are planned with extended response to 50 cm^{-1}. Many boron implanted BIB detectors have had problems with the boron not being active in spectral response measurements. This may be due to a high donor concentration in implanted layers.

The implanted layers have been characterized by Hall effect and DLTS. Cu has been shown to be a large contamination in the boron implanted layers. DLTS characterization of the implanted layer did not show a donor in p-type Ge, but a donor, E_c-0.335eV, in n-type Ge was observed. Cu was found in both types of detectors in large concentrations. Future projects will address the nature of the deep donor especially its relationship to Cu and/or residual ion implantation defects on BIB device performance.

II. Double Donor Studies

1. Introduction

Oxygen is one of the most studied impurities in silicon because of its high concentration in Czochralski grown silicon and its electrical properties. Based on this interest in oxygen, the other group VI elements have also been studied thoroughly (Wagner, et al. 1984). In germanium group VI impurities have been studied to a lesser degree (Grimmeiss, et al. 1988). A group VI impurity on a lattice site in a group IV crystal is expected to be a double donor with two levels in the band gap. Such a double donor can be modeled as a helium atom with a modified Rydberg coefficient in close analogy to the shallow hydrogenic impurities (Reuszer and Fisher 1964). Improved models also consider impurity ionization potentials, screening effects, and lattice relaxation to more accurately describe the double donor wavefunctions and energy levels. All the substitutional double donors in silicon show very deep ground state energies attributed to pronounced chemical shifts (Janzén, et al. 1984). Since sulfur is isochoric with silicon and has a large binding energy, one may speculate that the binding energy of selenium in germanium to be large also (Kohn, 1957).

Few researchers have performed studies of selenium in Ge, and these studies had limited success. Different energy levels have been measured depending on the doping technique. The accepted hypothesis for this disagreement has been that selenium has a tendency to form pairs and other complexes, a trend which has been shown for selenium in silicon (Janzén, et al. 1984). The tendency to form complexes increases with decreasing atomic radii of the dopant for chalcogens in silicon (Wagner, et al. 1984). Selenium in silicon has been shown to exist in three different states, substitutional, paired and

complexed (Janzén, et al. 1984). To accurately measure the donor energy levels due to the substitutional selenium, complex formation during doping must be suppressed. I have studied selenium impurity energy levels using a doping technique which minimizes complex formation. Neutron transmutation doping, to be described later, introduces selenium into germanium in a random distribution at low temperatures, inhibiting interaction between selenium atoms.

2. Review of Previous Work

2.1 Doping Techniques

2.1.1 Diffusion & Melt Doping

Many methods have been used to introduce electrically active selenium into Ge. The common technique is the diffusion of selenium that has been evaporated onto the surface. Some authors (Pearton 1982) report problems with the low solubility of selenium in Ge and the need for a cap of amorphous Ge on the selenium layer, because of the high selenium vapor pressure. High temperatures (750-800°C) are needed for diffusion, because of the low selenium diffusion coefficient. High temperature annealing promotes the diffusion of unwanted impurities into the crystal and enhances complex formation. Chalcogens in Si have been shown to form complexes (Janzén, et al. 1984). In Ge, at these high temperatures and concentrations, chalcogen interactions are likely and complex formation will occur upon cooling. Most authors have ignored this possibility in the analysis of their data (Tyler 1959; Pearton 1982).

A second doping technique, melt doping, has resulted in low concentrations of electrically active selenium centers (Tyler 1959). Low incorporation was attributed to the

high vapor pressure of selenium leading to the loss of the dopant from the melt. This method would also promote complex formation due to the high temperate of growth.

2.1.2 Neutron Transmutation Doping

Neutron transmutation doping (NTD) can be used for introducing selenium in germanium. NTD naturally leads to uniform doping of semiconductors. The process works by irradiating a semiconductor with thermal neutrons. Upon neutron capture, some of the newly formed isotopes will decay into doping elements. Because the distribution of isotopes is random and the absorption cross sections for thermal neutrons is very small, the doping is very homogenous through out the semiconductor sample. The concentration of dopants is given by the following equation.

$$N = A \bullet \rho \bullet n \bullet \sigma_c \bullet t_o \qquad [2.1]$$

In equation 2.1, A is the isotope fraction, ρ is the atom density of germanium (atom cm^{-3}), n is the neutron flux (cm^{-2} s^{-1}), σ_c is the neutron capture cross section (cm^2), and t_o is the irradiation time(s). The doping can be completely controlled by the irradiation time.

Isotopes	Abundance (%)	σ_c ($x10^{-24}$ cm^2)	Product	$T_{1/2}$	Type
^{70}Ge	20.5	3.25	^{71}Ga	11.2 d	p
^{72}Ge	27.4	1.0	^{73}Ge		
^{73}Ge	7.8	15.0	^{74}Ge		
^{74}Ge	36.5	0.52	^{75}As	82.2 m	n
^{76}Ge	7.8	0.16	^{77}Se	11.3, 38.8 hrs	n

Table 2.1 NTD parameters of natural Ge

Natural Ge consists of 5 stable isotopes with known abundance, as shown in Table 2.1. Ge is the only semiconductor that can produce both n and p type dopants by NTD. ^{70}Ge transforms to ^{71}Ga for p-type doping, and ^{74}Ge transforms to ^{75}As for n-type doping.

^{76}Ge after neutron capture produces ^{77}Se and 2 β-decays, in which electrons are ejected from the nucleus. For natural Ge, the amount of Se produced will be small compared to the production of Ga and As, due to the low abundance and low capture cross section of ^{76}Ge. Natural Ge will be p-type after thermal neutron irradiation which makes it difficult to observe the donor levels of selenium. Selenium is much more easily observed in n-type Ge. Isotopically enriched ^{76}Ge is a better candidate for selenium NTD studies, because the ^{76}Ge concentration can be increased, and the ^{70}Ge concentration can be decreased. The decay process for ^{77}Ge is shown in equation 2.2.

$$Ge^{76}(n,\gamma)Ge^{77} \xrightarrow{\beta-decay, T_{1/2}=11.3hrs} As^{77} \xrightarrow{\beta-decay, T_{1/2}=38.8hrs} Se^{77} \qquad [2.2]$$

After thermal neutrons have been captured by isotopes of natural Ge, decay products begin to appear. The total irradiation time, $t_o \sim 1$ hour, is small compared to the two half-lives of the ^{77}Ge decay series. Therefore we ignore the irradiation time when determining the start of the decay time. ^{71}Ge half-life, 11.2 days, is also much longer than the irradiation time. ^{75}Ge is different than the past two decay series, because the half-life, 82 minutes, is comparable to the irradiation time and decay products will be produced rapidly.

The concentration of isotopes after thermal neutron irradiation can be determined. The radioactive isotopes decay exponentially time, $N_r=N_o\exp(-\lambda t)$, where λ is a constant. N_r is the concentration of remaining radioactive nuclei, and N_o is the initial concentration

of radioactive nuclei. The half-life is the time required for the initial concentration to drop to half of its value. To determine the decay rate in terms of half-life, N_r is set at half the initial concentration.

$$N_r = 0.5N_o = N_o \exp(-\lambda T_{1/2}) \qquad [2.3]$$

We find $\lambda T_{1/2} = \ln 2$. The concentration of daughter isotopes produced, N, is the initial concentration of radioactive nuclei, N_o, minus the remaining nuclei, N_r.

$$N = N_o - N_r \qquad [2.4]$$

The concentration of daughter isotopes produced, N, is

$$N = N_o[1 - \exp(\frac{-t \ln 2}{T_{1/2}})] \qquad [2.5]$$

where t is the time after irradiation. The growth of the intermediate As concentration and the final selenium product are shown in Fig. 2.1. After irradiation, ^{77}Ge starts to decay

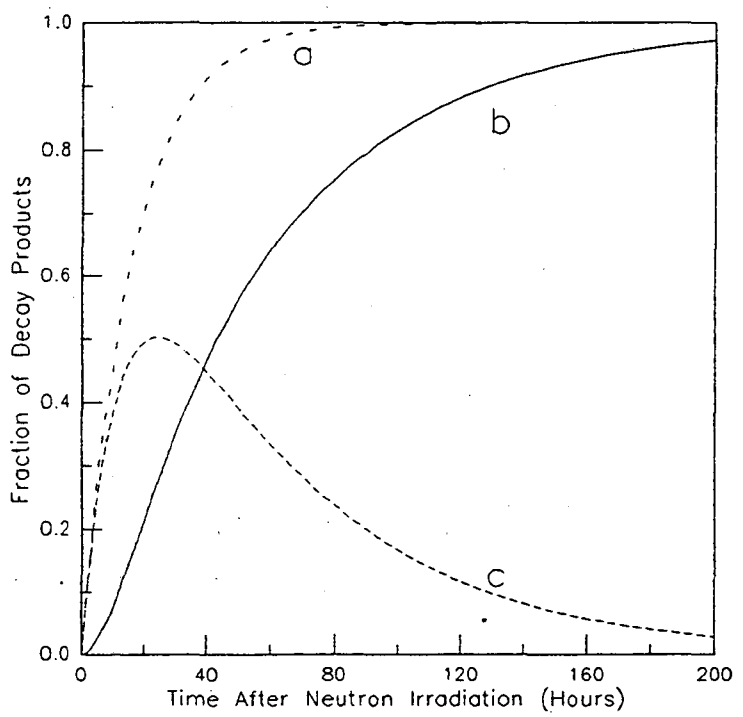

Fig. 2.1 a) Fraction of As transformed, b) Fraction of Se transformed, c) Concentration of As

into ^{77}As. This progresses much faster than the subsequent ^{77}Se formation, because of the large difference in half-lives. The progress with time of the selenium concentration can be described by the following equation and is shown in curve b Fig. 2.1.

$$N_{Se} = N_{As}[1-\exp(\frac{-t\ln 2}{38.8hrs})] = N_o[1-\exp(\frac{-t\ln 2}{11.3hrs})][1-\exp(\frac{-t\ln 2}{38.8hrs})] \qquad [2.6]$$

A disadvantage of the NTD technique is the production of radiation damage due to fast neutrons, fission gamma rays, gamma ray recoil, beta recoil, and charged particle knock-on.

Of these we only consider fact neutron damage and beta recoil. The other sources are much less important (Larrabee 1984). The β-decay process transfers kinetic energy to the atom which may knock the atom of its lattice site. The maximum energies of the electron emitted in the first ^{77}Ge beta decay are 2.196 MeV (42% of the time), 1.379(35%), and 0.71(23%) (Browne, et al. 1978). The 2.196 MeV β-particle keeps most of its energy and transfers a maximum energy of 196 eV to ^{77}As atom. This maximum transferred energy T_{max} can be calculated using the relativistic correction to the momentum transfer (Kelly and Groves 1970).

$$T_{\max} = \frac{2E(E+2mc^2)}{Mc^2} \qquad [2.7]$$

In this equation, M is the mass of the lattice atom, m is the electron rest mass, E is the kinetic energy of the electron, and c is the speed of light. This energy is much larger than the displacement energy of 20 eV needed to knock the ^{77}As atom off its lattice position. Because in β-decay two particles are formed, an electron (β-particle) and an electronic antineutrino $\bar{\nu}_e$, the β-particles emitted have a distribution of energies below the maximum

energy. The Fermi-Kurie plot describes the energy distribution for the three body interaction. It was calculated for the β-particle distributions shown in Fig. 2.2. One sees that on average the energy of the β-particle is only about 1/4 of the maximum energy and the energy transferred to the ^{77}As as calculated by equation 2.6 is correspondingly lower. Probabilities of atoms knocked off their lattice sites by β-particle recoils will be shown in a later section. The β-particle for the second decay has an energy of 0.70 MeV. The maximum transferred energy to the ^{77}Se is 33eV. Therefore the second β-decay has a much lower probability of producing lattice disorder.

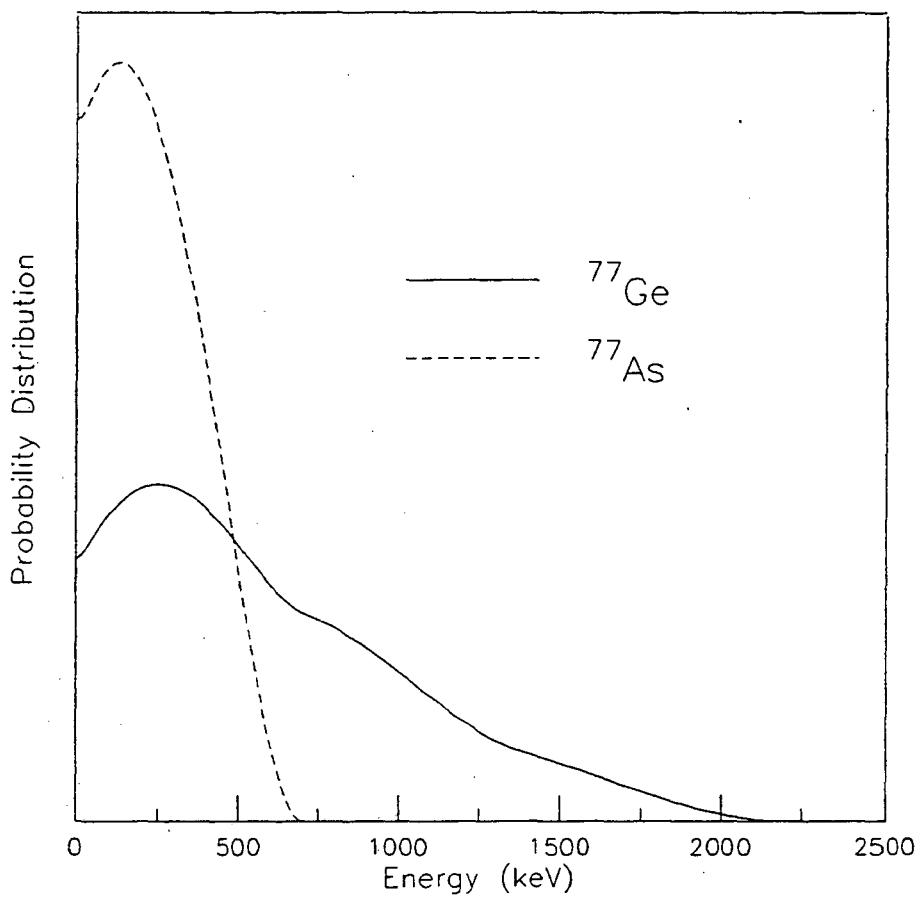

Fig. 2.2 Energy distribution of β-particles

After neutron irradiation, fast neutron and beta recoil damage are removed by annealing. Annealing is necessary to remove deep level defects generated. Complete recovery occurs after 6 hours of annealing at 400°C (Palaio, et al. 1984). I.S. Park showed that small residual concentration of deep level defects are stable even up to annealing temperatures of 700°C for 1 hour (Park 1988).

Another advantage of NTD is the perfect control of the dopant concentration. The selenium dopant concentration is directly proportional to the total thermal neutron dose. The dose is the flux times irradiation time. If low neutron doses, 10^{16} cm^{-2} are used, the individual selenium dopant atoms are far apart, due to the low concentration. Since NTD is done near room temperature, there is no chance for the selenium to diffuse and to form complexes during NTD.

2.2 Characterization of Energy Levels

Tyler was the first to diffuse selenium and other chalcogens into germanium and measure their energy levels (Tyler 1959). He diffused Se into Ge in quartz ampoules at 920°C and added it to melt-doped crystals. He measured the diffusivity to be very low, $\sim 10^{-10}$ cm^2/sec at 920°C. Tyler measured these levels with variable temperature Hall effect, which is not as sensitive for deep levels as Deep Level Transient Spectroscopy (DLTS). Tyler observed two levels at E_c-0.14eV and E_c-0.28eV. He measured different concentrations for each level, which indicated that they do not belong to the same impurity or that his samples were partially compensated. The concentration for the 0.28eV level was several times greater than the 0.14eV level for both melt-doped and diffused Ge crystals.

Pearton(Pearton 1982) did a systematic study of many impurities in germanium by diffusing them in at 750°C and performing DLTS. Pearton found selenium donor levels to be at E_c-0.11eV and E_c-0.30eV in n-type material, and found an acceptor at E_v+0.05eV in p-type material. The two donor levels showed similar concentrations, indicating that they might belong to the same impurity. Pearton determined the diffusion constant for Se to be $8\pm4\times10^{-12}$ cm^2/s at 750°C.

Grimmeiss diffused selenium into Ge at 765°C. His group performed a very comprehensive study by using optical absorption spectroscopy and DLTS techniques. For one deep level, Grimmeiss and Pearton measured similar activation energies of E_c-0.284 eV and E_c-0.30eV, respectively (Grimmeiss, et al. 1988). Pearton believed that this was the second level of selenium, while Grimmeiss' IR spectroscopy results suggested that it should be the first energy level. From the spacing of excited states in the absorption spectrum, Grimmeiss inferred that the E_c-0.268eV level, must correspond to neutral selenium. The E_c-0.268eV level is assumed to be the same level as the E_c-0.284 eV activation energy obtained by DLTS which must be corrected for the entropy. This indicates that the E_c-0.11eV level measured by Pearton must belong to a shallower Se complex or another impurity.

Osip'yan, et al., used NTD of natural germanium to dope with selenium (Osipyan, et al. 1984). Shortly after irradiation and annealing, the material was n-type due to arsenic formation from ^{74}Ge, which has a half-life of 82 minutes. The half-life for ^{70}Ge transmuting into gallium is 11.2 days, so the germanium changed from n-type to p-type only after 6 days. After the As is formed, selenium will form before the Ga. By measuring

the electron and hole concentrations with Hall effect as a function of time, Osip'yan et al., determined the effect on the total carrier concentration of the selenium donors as they appeared. The selenium concentration was small, because ^{76}Ge has a small capture cross section and a small abundance in natural Ge. The selenium contribution to the carrier concentration is low at room temperature, because the deep levels are only partially ionized. Osip'yan deduced from variable temperature Hall effect that only the E_c-0.28eV level is due to the substitutional Se. The E_c-0.11eV level measured by Pearton, was not observed by this doping technique.

2.3 Neutron Damage

The disadvantage of NTD is the production of large defect clusters as well as isolated point defects caused mainly by fast neutrons. V. Nagesh and J. W. Farmer (Nagesh and Farmer 1988) did a systematic study of γ- and neutron-irradiation defects in phosphorus, antimony and oxygen doped Ge crystals. They found 4 electron traps: the planar-four vacancy at E_c-0.09eV, the divacancy at E_c-0.17eV, the vacancy-oxygen (analog of E center in Si) pair at E_c-0.27eV, and the donor-vacancy (analog of A center in Si) pair at E_c-0.35eV. The concentration of all four of these electron traps decrease after annealing between 100°C and 200°C for 30 minutes. The E_c-0.35eV level produced was dominant in the spectrum, but is not the selenium level, because Nagesh et al., observed the level in γ-irradiated as well as neutron-irradiated crystals.

After irradiation, the group V shallow impurities become compensated. The low electrical activity after irradiation has been studied for many of the group V impurities in germanium (Emtzev, et al. 1972). The simplest explanation is the creation of

compensating acceptors. This was negated by Emtzev, et al., who showed by Hall effect that the decrease in shallow donors is greater than the increase in compensating acceptors after irradiation. Another possibility is the trapping of vacancies by shallow donors forming neutral complexes. This explains the absence of electrically active donors. From low temperature irradiation studies, it is known that vacancies are mobile well below room temperature and thus can travel to donor sites. This model has found strong support by far IR spectroscopy measurements performed by Park and Haller. They showed that while Ga acceptors were present in as doped material, no donor transitions could be observed after neutron irradiation. Only after annealing the As donors become active (Park 1988).

3. Impurity Identification Through Isotope Engineering

NTD of natural Ge leads to a relatively small concentration of selenium compared to the Ga and As concentrations. NTD of crystals with an artificially increase atomic concentration of ^{76}Ge will lead to larger relative concentrations of selenium. By controlling the ratio of ^{74}Ge to ^{76}Ge isotopes in a crystal, the final concentration of Se can be deliberately "engineered" to be about 10% of the final As concentration. To control the Se to As ratio, the thermal neutron capture cross sections of ^{74}Ge and ^{76}Ge must be taken into account when determining the isotope ratio with isotope engineering.

3.1 Growth of Small Crystals

Due to the limited availability and high cost of isotopically enriched Ge, K. Itoh of our group developed a technique for growing small, isotopically pure as well as mixed germanium crystals of about 4 grams by the vertical Bridgman method (Itoh 1992). In the

vertical Bridgman method the germanium is melted in a graphite crucible and then exposed to a vertical temperature gradient. The crystal nucleates at the bottom usually in a <113> orientation and growth obeys normal freeze. The system was designed to be seedless to preserve the isotopic purity.

3.2 NTD Isotopically Enriched Ge

A $^{74/76}$Ge crystal was grown by K. Itoh with an isotope mixture of ^{70}Ge (0.4%), ^{72}Ge(0.2%), ^{73}Ge(1.7%), ^{74}Ge(76.1%), and ^{76}Ge(21.6%) as measured by SIMS. The isotopic fractions of ^{74}Ge and ^{76}Ge should produce n-type Ge with a Se to As ratio of 8.7:100 after NTD. NTD was performed by John Farmer at the research reactor at the University of Missouri. Processing of Ge for characterization occurred after NTD. Diodes were prepared by implanting boron at room temperature for the rectifying contact and phosphorus at liquid nitrogen temperatures to form the ohmic contact. The phosphorus contact was annealed in a 15 hour temperature ramp from 50°C to 330°C. After this annealing ramp, the bulk material was p-type, because deep acceptors were introduced by neutron damage and the arsenic was still compensated by vacancies. Higher temperature anneals at 400°C were needed to transform the Ge to n-type activating the arsenic.

3.3 Characterization

3.3.1 Deep Level Transient Spectroscopy (DLTS)

DLTS, described in section I chapter 2.3.5, is the most sensitive technique for studying deep levels at low concentrations.

Producing ^{77}Se by NTD has the disadvantage of leading to radiation damage in the material and compensation of the shallow donors. The fast neutrons and β-decay recoils

introduce deep levels into the gap that can complicate the Se identification. In order to avoid such complications, we fabricated a reference sample. The DLT spectrum of neutron irradiated n-type ^{74}Ge should show only deep levels associated with neutron damage and residual impurities, because ^{74}Ge produces only shallow arsenic levels. The n-type $^{74/76}$Ge should show the same levels in the DLT spectrum, plus additional levels related to selenium.

The diodes in Fig. 3.1 were annealed to transform the samples to n-type by activating the arsenic at 400°C for 1 hour. Diodes were measured at τ=35 ms, 1.0 ms

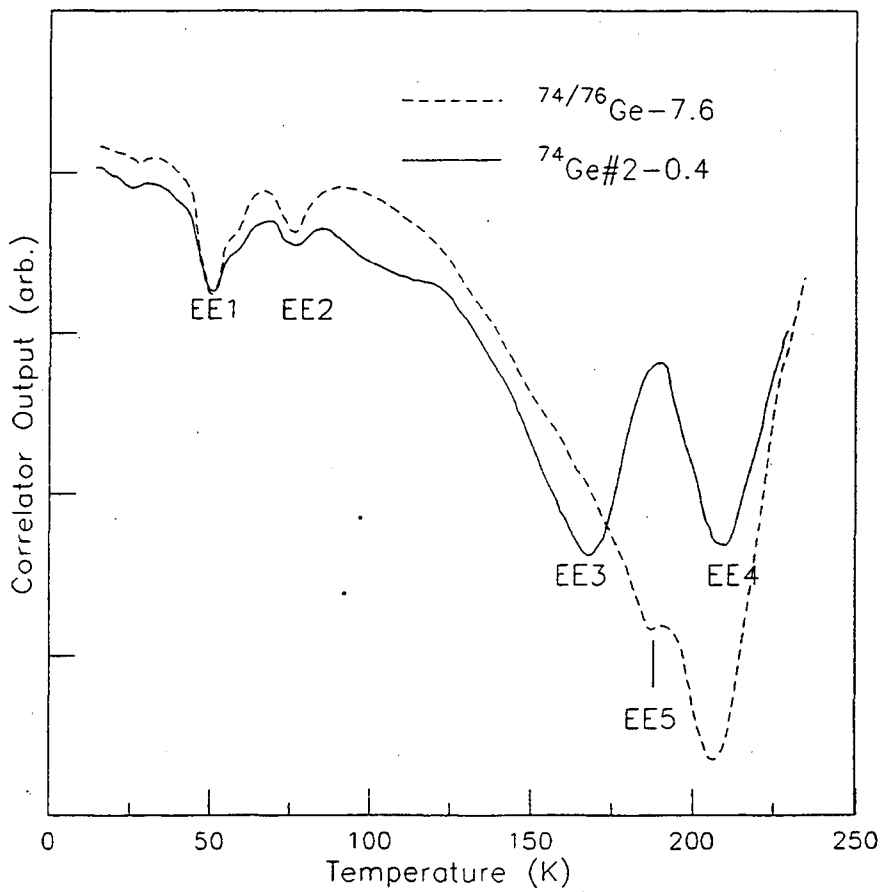

Fig. 3.1 DLTS of ^{74}Ge and $^{74/76}$Ge after neutron irradiation and annealing at 400°C for 1 hour.

pulse width, and 1.5 ms holdtime after the beginning of the pulse. The fixed bias was 4.0V and the pulse was 2.0V. Both samples received a neutron dose of 2.4×10^{16} cm^{-2}, so they should have similar amounts of damage. Electron traps are labeled with EE# nomenclature.

The ^{74}Ge diode spectrum showed four deep levels, EE1 through EE4, attributed to irradiation damage. The $^{74/76}Ge$ diode spectrum contained the same deep levels as the ^{74}Ge, plus an additional deep level EE5 with an activation energy of 0.325eV that can be related directly to selenium.

The EE3 deep level appears to have similar concentrations in both samples, but the EE4 deep level is much larger in the $^{74/76}Ge$ sample. Speculation that a second selenium deep level is at the same position as EE4 has little support at the moment and we are planning further experiments to test this point.

The ^{74}Ge and $^{74/76}Ge$ diodes had turned from p-type to n-type after one hour annealing at 400°C. The activated arsenic fraction was 52.0% for the $^{74/76}Ge$ sample and 50.5% for the ^{74}Ge sample after 1 hour determined by C-V measurements. After a second hour of annealing at 400°C, these fractions rose to 55.0% and 56.1%, respectively. The DLT spectrum after the second hour of annealing is in Fig. 3.2.

The EE5 selenium deep level has annealed away faster than the neutron damage. The deep level is still present in the background of the $^{74/76}Ge$ sample compared to the background level of the ^{74}Ge sample. Further analysis of this Se related peak is extremely difficult, because it is at lower concentrations compared to the surrounding deep levels.

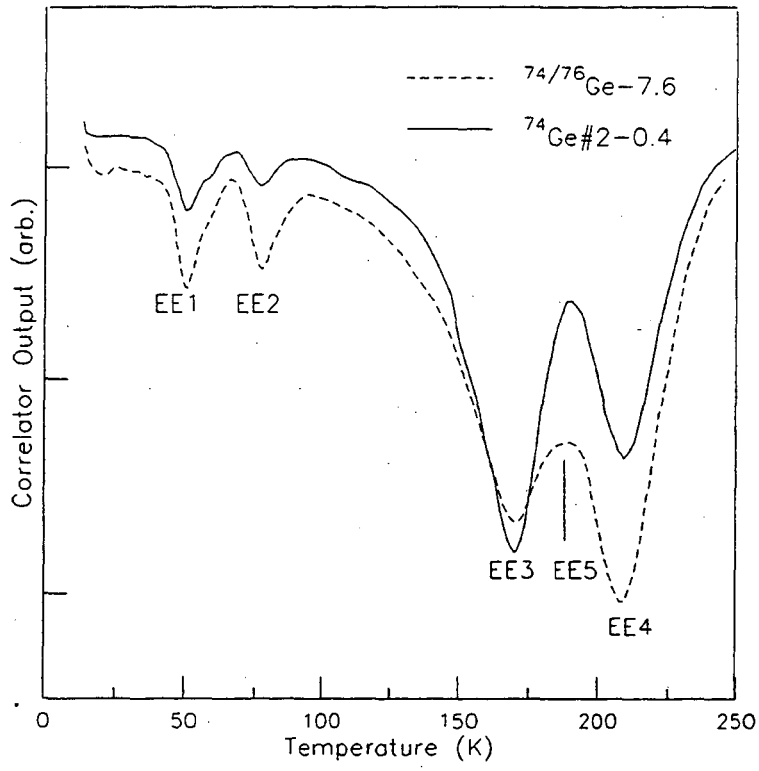

Fig. 3.2 DLTS of ^{74}Ge and $^{74/76}$Ge after neutron irradiation and annealing at 400°C for 2 hours

The deep level data associated with ^{74}Ge and $^{74/76}$Ge are in Table 3.1. The EE1-4 traps were also observed in the $^{74/76}$Ge sample. τ is the inverse of the emission rate. The temperature corresponds to the emission rate of each trap. An Arrhenius plot of $\ln(1/\tau T^2)$

τ	^{74}Ge EE1	^{74}Ge EE2	^{74}Ge EE3	^{74}Ge EE4	$^{74/76}$Ge EE5
5ms	57 K	86 K	182 K	228 K	207 K
12ms	54 K	82 K	176 K	221.5 K	197 K
35ms	50.5 K	76 K	168 K	209 K	188 K
120ms	47K	72 K	160.5 K	198.5 K	178.5 K
E_a(meV)	64	104	339	370	325
R^2	0.9998	0.991	0.999	0.992	0.997

Table 3.1 DLTS Data for Majority Traps in ^{74}Ge and $^{74/76}$Ge

vs. 1/T gives a slope proportional to the activation energy, E_a, of the deep level. R^2 is the quality of the linear regression fit. The data is more linear for R^2 closer to one.

3.3.2 Isothermal Annealing Behavior

Another $^{74/76}$Ge sample has been irradiated, but without a reference ^{74}Ge sample. The $^{74/76}$Ge-7.2 sample received a neutron dose of 5.4×10^{15} cm^{-2} and was annealed at a higher temperature for various times. The final dopant concentrations calculated by equation 2.1 for set 7.2 were [As]=$9.36 \times 10^{13} cm^{-3}$ and [Se]=8.18×10^{12} cm^{-3}. The sample was annealed at 450°C for 1, 2, and 4 hours. Electron traps are labeled with the E# nomenclature. The DLT spectra for a $^{74/76}$Ge diode from set 7.2 are shown below in Fig. 3.3 and the activation energy data are given in Table 3.2. The measurement parameters for the diode shown in Fig. 3.3 were τ=35ms, 1.8ms holdtime, 0.8ms pulse width, 1.0V bias, and 0.8V pulse.

τ	E1	E2	E3	E4
5ms	63.5 K	83 K	123.5 K	184 K
12ms	61 K	79 K	116 K	178 K
35ms	59 K	77 K	113 K	172 K
120ms	56.5 K	73 K	107 K	163 K
E_a(meV)	132	157	205	364
R^2	0.996	0.98	0.97	0.993
$\sigma(cm^2)$	9.1×10^{-13}	6×10^{-14}	2×10^{-15}	2.9×10^{-14}

Table 3.2 DLTS Data for Majority Traps in $^{74/76}$Ge-7.2

The selenium level EE5 is not apparent after 1 hour annealing at 450°C. The concentration of the E2 deep level increased after annealing at 450°C and has similar emission rates as EE2 in the ^{74}Ge sample. Therefore it is most likely the same level and is

related to neutron damage, not selenium complexes forming. The E4 deep level is very similar to the EE3 level in the ^{74}Ge sample and therefore is most likely caused by neutron damage.

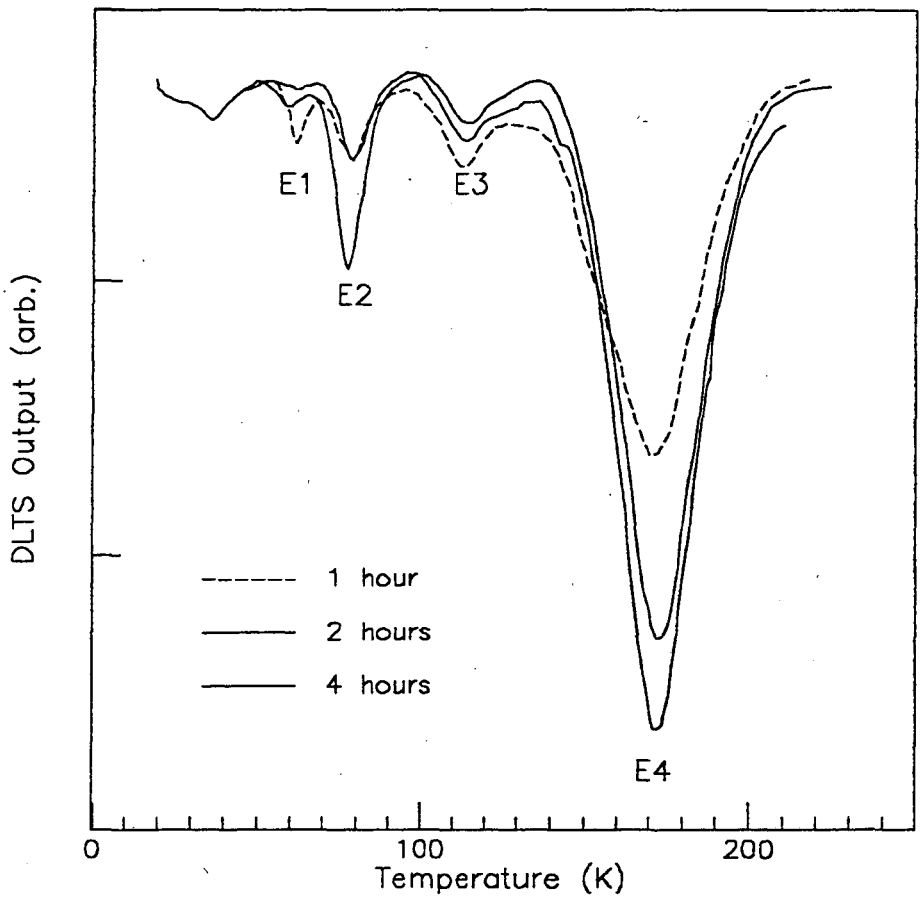

Fig. 3.3 DLTS of $^{74/76}Ge$-7.2 after annealing at 450°C

In the process of identifying the unknown deep levels, it is important to compare known strong contaminants. Cu is known to be a likely contaminant in Ge. As a reference, Cu was diffused into a n-type Ge crystal 831-15.8. DLTS was performed to determine the emission rates of electron capture by the third acceptor level of substitutional $Cu^{2-/3-}$. The activation energy was measured to be 345meV which agreed

reasonably well with data in the literature of 325 meV (Clauws, et al. 1989). Measured inverse emission rates in Table 3.3 are for the third level of Cu.

τ	$Cu^{2-/3-}$
5ms	186K
12ms	178.5 K
35ms	172 K
120ms	163.5K
E_a(meV)	345
R^2	0.99

Table 3.3 Electron capture by third acceptor level of Cu in n-Ge

After irradiation with neutrons, vacancies bond to the arsenic atoms and passivate them. Park and Haller showed that with IR absorption, arsenic dopants were passivated until annealed (Park 1988). Annealing breaks the arsenic-vacancy complexes, and the shallow arsenic concentration increases with annealing time, as shown in Fig. 3.4.

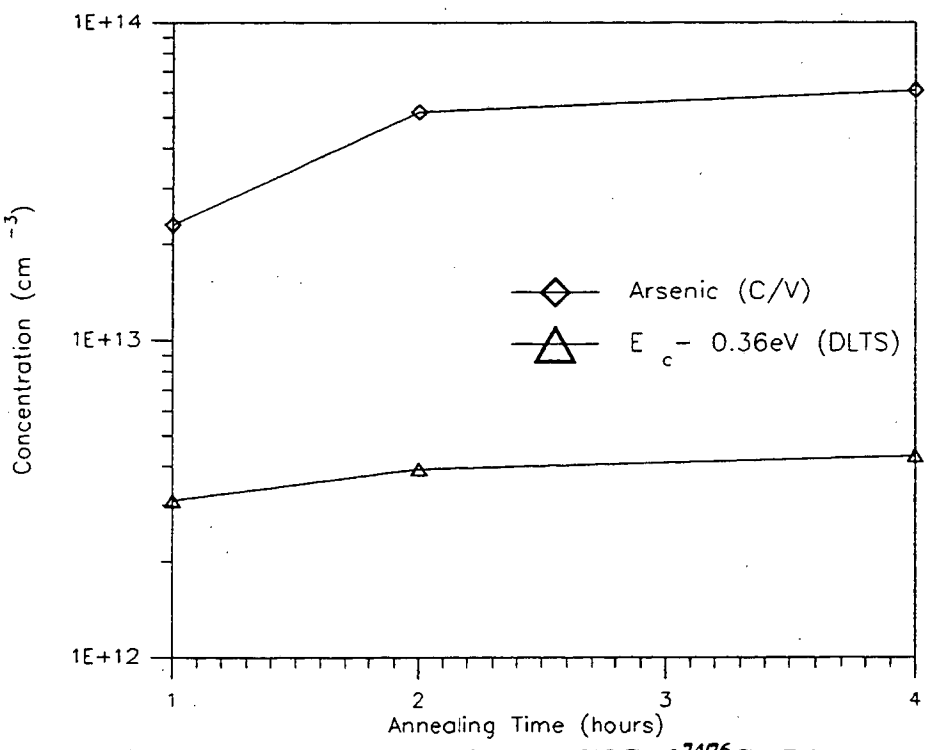

Fig. 3.4 Isothermal Annealing at 450°C of $^{74/76}$Ge-7.2

The EE3 and E4 levels have very similar emission rates and activation energies compared to $Cu^{2-/3-}$. Cu may be activated at a higher rate, because the Fermi level is shifting up as the Ge becomes more n-type. The Cu could originally come from the depassivation of the CuH_3 centers or from Cu precipitates at dislocations. The activation of Cu acceptors in n-type Ge is driven by a decrease in total energy. Compensating species introduce levels lower in the gap. Electrons from shallow donors fall into these states and the total energy of the system decreases.

The As concentration in the $^{74/76}$Ge sample shows the same increase in concentration as the E4.(Fig. 3.4) This implies that with the Fermi level rising in the Ge crystal, more Cu becomes active.

3.3.3. Absorption Spectroscopy

IR absorption was performed on $^{74/76}$Ge-7.2 samples to verify the presence of selenium energy levels at 0.325eV and 0.268eV. The first level was seen by DLTS in our samples. The second level was observed by Grimmeiss in diffused Ge:Se samples in IR absorption and DLTS. Our absorption measurements were done with a Digilab spectrometer with a Ge:Cu photoconductive detector. The estimated selenium concentration for the sample was 8.2×10^{12} cm^{-3}. No IR absorption was observed at 268 meV or at 360 meV. An excitation directly from the deep level at specific k-vector to the conduction band has a low probability, and the concentration was most likely too produce measurable absorption from a deep level.

4. Selenium Melt Doped Germanium

Selenium melt doped crystals were also characterized with DLTS to the NTD selenium doped Ge crystals. Czochralski crystals have been grown with the introduction of selenium into the melt by W. Hansen at the Lawrence Berkeley Laboratory. A large concentration of selenium was added to the melt, but the electrical concentration was low compared to the actual physical quantity added. Variable temperature Hall effect showed a shallow electrical activity of 1.5×10^{13} electrons cm^{-3} at 200K. Secondary ion mass spectrometry (SIMS) was performed to detect the physical atoms of selenium, in case the selenium is incorporated into the melt, but is electrically inactive. No selenium was found above the SIMS background limit of $\sim 10^{15}$ cm^{-3}.

Selenium may have a very low solubility limit in Ge. To overcome the low solid solubility limit, a n-type melt doped sample was quenched from 400°C to room temperature after 1 hour annealing to freeze the selenium on substitutional sites. The n-type sample was sealed in an ampoule with in 1/2 atm of argon gas. Before quenching, the shallow net donor concentration was $1.1 \times 10^{13} cm^{-3}$ measured by C/V at 180K. After quenching the shallow net donor concentration fell to $4.5 \times 10^{12} cm^{-3}$ at 180K. The drop in free carrier concentration could be due to activation of compensating copper acceptors. DLTS was performed both on the slowly cooled sample and the sample quenched from 400°C. The spectra are shown in Fig. 3.5. The samples were measured at τ=35ms, 1.0ms pulse width, and 1.5ms holdtime. The fixed bias was 2.0V and the pulse bias was 0.75V. The spectra in Fig. 4.1 are corrected for difference in shallow concentration of the two

samples. M# is used for the nomenclature of the slowly cooled sample and Q# is used for the quenched sample. The two S-87 samples have both been verified to be n-type bulk, by collecting α-particles through a p-type rectifying contact.

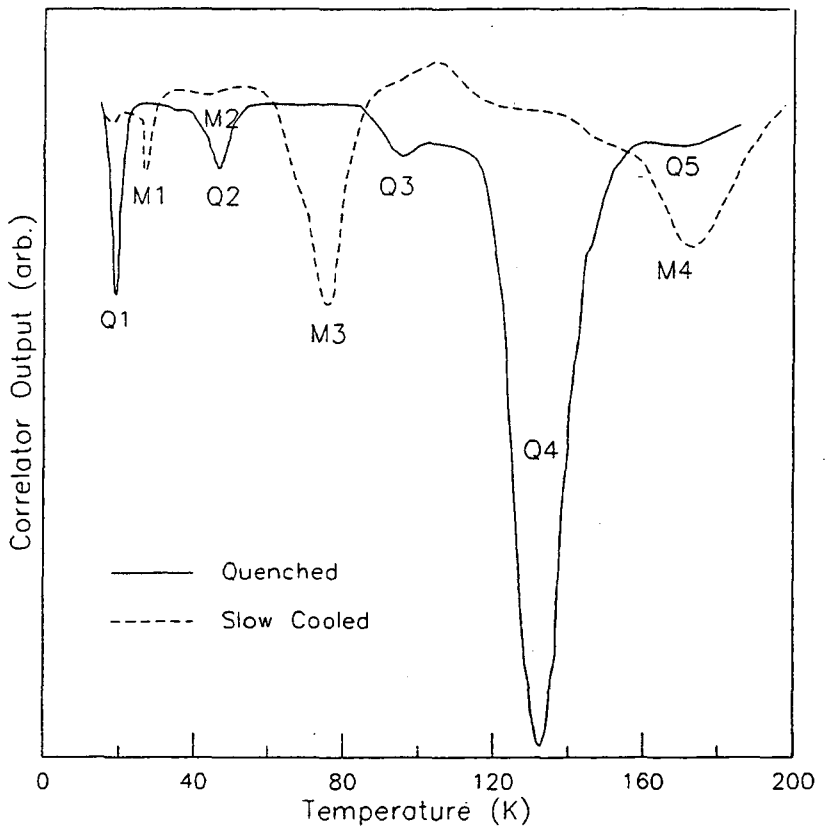

Fig 4.1 S-87 Ge:Se Melt Doped

The radical change in the spectrum cannot be explained at this moment. Deep levels M2 and Q2 have similar activation energies and emission rates and are most likely due to the same center. Deep levels M4 and Q5 also have similar activation energies and emission rates and are most likely the same level. The levels in the melt doped samples could not be correlated with any of the levels from the NTD samples.

5. Discussion

A deep level at 0.325 eV has been measured in the NTD $^{74/76}$Ge sample that can be attributed only to selenium, because of its absence in the ^{74}Ge reference sample. With the use of NTD and a low annealing temperature, the selenium interactions are reduced. The use of NTD increases the probability that the selenium atoms occupy substitutional sites, because the ^{76}Ge atoms originally occupied substitutional sites before it became selenium. Therefore, I tentatively assign this energy level to selenium on a substitutional site. We notice that the stability upon thermal annealing of this level is extremely low.

Only one deep level could be attributed to selenium. A selenium impurity, however, should act as a double donor and so two energy levels should be present. No other peak of similar concentration was apparent in the upper half of the gap. The other energy level may be in the lower half of the gap, which is more difficult to examine. To probe the lower half of the gap, DLTS was done under injections conditions. No hole traps were observed. The trapping of a hole by a positively charged center, a donor, is a repulsive and weak process. The strong electron traps dominating the spectrum may have masked the minority trap signal if it exists.

6. Future Work

To be able to measure a donor in the lower half of the band gap, the material must be extremely defect-free except for the levels under investigation. I plan to anneal a NTD Ge sample immediately after irradiation, so that the fast neutron damage is removed before all the ^{77}Ge radioactive isotopes decay into Se. The β-decay recoil of the ^{77}Ge to ^{77}As transformation may produce lattice damage, so the sample is to be annealed when

difference between the fraction transformed of ^{77}As and ^{77}Se is the largest. This occurs at 24.5 hours after irradiation, when the 78% of the ^{77}As has transformed but only 28% of the ^{77}Se has formed. Annealing at this time will minimize the lattice damage and selenium complex formation. This will allow the study of the selenium levels without so many interfering damage levels. There is still the small possibility of selenium displacement by electron recoil upon emission of the β-particle.

The threshold of an electron with enough energy to cause displacement in Ge is approximately 450 keV, but the damage threshold is not sharp. A range of displacement energies was used in calculating the percentage of β-particles that do not knock the atom off its lattice site, shown in Table 6.1.

Displacement Energy	^{77}Ge	^{77}As	Se_s for annealing at t = 24.5 hrs	Se_s: for annealing at t = 0 hrs
300keV	29.2%	67.0%	37.8%	19.6%
450keV	44.0%	89.8%	53.6%	39.5%
600keV	56.3%	99.2%	61.9%	55.8%

Table 6.1 Percentage of β-particles that do not have enough energy to dislodge the host atom from its lattice site.

The energy distribution of the β-particles is known and was shown in Fig. 2.2. These values allow the calculation of the percentage of selenium atoms that occupy substitutional sites after annealing at 24.5 hours after irradiation and immediately after irradiation. More selenium ends up on substitutional sites by annealing at 24.5 hours than immediately after the irradiation, because of the recovery of ^{77}As back on to lattice sites.

The sample will be investigated with DLTS and PTIS to find the other selenium energy level and better characterize the E_c-325 meV level already observed.

7. Conclusion

Selenium in Ge has been studied with a doping technique which limits complex formation. Only one ionization level has been found to correspond to selenium, which presumably occupies a substitutional site. This level is extremely unstable and its concentration decreases after annealing at 400°C. Future work is planned to anneal the fast neutron damage before much selenium has formed in the $^{74/76}$Ge samples. It is expected that the observed selenium level can be better characterized and the missing selenium level is more likely to be discovered if other defects are removed before ^{77}Se formation.

III References:

B.A. Andreev, G.G. Devyatykh, V.A. Gavva, D.M. Gordeev, A.V. Gusev, G.A. Maksimov, V.G. Pimenov, V.B. Shmagin and D.A. Timonin, Semicond. Sci. Technol. **9**, 1050 (1994).

R.J. Bell. *Introductory Fourier Transform Spectroscopy* (Academic Press, New York, 1972).

P.R. Bratt, in *Semiconductors and Semimetals*, edited by R.K. Willardson and A.C. Beer (Academic Press, New York, 1977), p. 39.

E. Browne, J.M. Dairiki and R.E. Doebler. *Table of Isotopes* 264 (John-Wiley & Sons, New York, 1978).

P. Clauws, G. Huylebroeck, E. Simoen, P. Vermaercke, F. DeSmet and J. Vennik, Semicond. Sci. Technol. **4**, 910 (1989).

L. Csepregi, R.P. Kullen, J.W. Mayer and T.W. Sigmon, Solid State Communications **21**, 1019 (1977).

V.V. Emtzev, T.V. Mashovetz and S.M. Ryvkin. 17 (University of Reading, 1972).

C.S. Fuller and J.C. Severiens, Phys. Rev. **96**, 21 (1954).

H.G. Grimmeiss, L. Montelius and K. Larson, Phys. Rev. B **37**, 6912 (1988).

N.M. Haegel. *Performance and Materials Aspects of Ge:Be and Ge:Ga Photoconductors for Far Infrared Detection* (UCB, 1983).

R.N. Hall and J.H. Racette, J. Appl. Phys. **35**, 379 (1964).

E.E. Haller, Infrared Physics **25**, 257 (1985).

E.E. Haller, M.R. Hueschen and P.L. Richards, Appl. Phys. Lett. **34**, 495 (1979).

W.L. Hansen, E.E. Haller and P.N. Luke, IEEE Trans. on Nuclear Science **NS-29**, 1 (1982).

K. Itoh. *Growth and Characterization of Isotopically Enriched ^{70}Ge and ^{74}Ge Single Crystals* (UCB, 1992).

E. Janzén, R. Stedman, G. Grossman and H.G. Grimmeiss, Phys. Rev. B **20**, 1907 (1984).

K.S. Jones. *Ion Implantation of Boron in Germanium* (UCB, 1985).

J.M. Kahn. *Hydrogen-Related Acceptor Complexes in Ge* (UCB, 1986).

A. Kelly and G.W. Groves. *Crystallography and Crystal Defects* 282 (Tech Books, Herndon, VA, 1970).

W. Kohn. *Solid State Physics* 257 (Academic Press Inc., New York, 1957).

D.V. Lang, J. Appl. Phys. **45**, 3014 (1974).

R.D. Larrabee. *Neutron Transmutation Doping of Semiconductor Materials* 336 (Plenum Press, New York, 1984).

D. Lecrosnier, Nuclear Instruments and Methods **209/210**, 325 (1983).

T.M. Lifshits, N.P. Likhtman and V.I. Sidorov, Soviet Physics-J.Exper.Theor. Phys. Letter **7**, 2076 (1968).

G.L. Miller, J.V. Ramirez and D.A.H. Robinson, J. Appl. Phys. **46**, 2638 (1975).

V. Nagesh and J.W. Farmer, J. Appl. Phys. **63**, 1549 (1988).

Y.A. Osipyan, V.M. Prokopenko and V.I. Tal'yanskii, JETP Lett **39**, 149 (1984).

M. Ozeki, K. Kitahara, K. Nakai and A. Shibatomi, Jap. J. Appl. Phys. **16**, 1617 (1977).

N.P. Palaio, S.J. Pearton and E.E. Haller, J. Appl. Phys. **55**, 1437 (1984).

I.S. Park. *Characterization and Application of Neutron Transmutation Doped Germanium* (UCB, 1988).

L.J. van der. Pauw, Philips Res. Rep. **13**, 1 (1958).

S.J. Pearton, Solid State Electron. **25**, 499 (1982).

R.H. Pehl, Nuclear Instr. & Methods in Phys. Research Section A **A242**, 103 (1985).

M.D. Petroff and M.G. Stapelbroek, IRIS Specialty Group on IR Detectors **Seattle,WA**, (1984).

G. Pilbratt, Infrared Phys. Tech. **35**, 407 (1994).

J.H. Reuszer and P. Fisher, Phys. Rev. **135**, 1125 (1964).

G.H. Rieke, M.W. Werner, R.I. Thompson, E.F. Becklin, W.F. Hoffman, J.R. Houck, F.J. Low, W.A. Stein and F.C. Witteborn, Science **231**, 807 (1986).

H. Ryssel and I. Ruge. *Ion Implantation* 459 (John Wiley & Sons, Chichester, 1986).

N. Sclar, Infrared Physics **16**, 435 (1976).

W.W. Tyler, J. Phys. Chem. Solids **8**, 59 (1959).

P. Wagner, C. Holm and E. Sirtl. *Chalcogens as Point Defects in Silicon* 191 (1984).

H.H. Woodbury and W.W. Tyler, Phys. Rev. **105**, 84 (1957).

I.C. Wu, J.W. Beeman, P.N. Luke, W.L. Hansen and E.E. Haller, Appl. Phys. Lett. **58**, 153 (1991).

F.X. Zach, Materials Science Forum **83-87**, 245 (1992).

Appendix A: Processing of Ion Implanted BIB Detector

The processing steps for the boron implanted BIB detector first tested by I.C. Wu is described. The BIB detector is fabricated out of germanium grown by the Czochralski method. The germanium is grown in an H_2 ambient from a SiO_2 crucible within a graphite susceptor. Material grown by this technique has between 10^{10} cm^{-3} and 10^{11} cm^{-3} residual net-dopant impurities. A wafer, approximately 1 mm thick, is cut from the boule. The material is lapped with #600 Al_2O_3 grit on both sides, washed and lapped with #1900 Al_2O_3 grit on both sides to remove mechanical damage from diamond saw cutting. The wafer is polish etched in HNO_3:HF:red fuming HNO_3 in the ratio of 7:2:1 to remove the lapping damage. One side is implanted with a series of boron implants at different energies, so they add up to a constant doping profile with a concentration of $3x10^{16}$ cm^{-3}. The lowest energy implant near the surface is given a higher dose to produce a degenerate p^+ contact layer. The wafer is sequentially cleaned in boiling trichloroethane, acetone, and methanol to remove the wax that held the sample down for ion implantation and other organics. A 10% KCN in H_2O soak for 2 minutes reduces the surface concentration of Cu and it is rinsed off with distilled H_2O. Annealing is performed at high temperature (typically 450°C) in an argon or reducing (N_2 + 4% H_2) gas ambient to anneal out implantation defects and to activate the boron. The temperature chosen for annealing is very crucial in regard to the defects that are annealed, while undesirable impurities diffuse in. After annealing, the native oxide is removed with 5%HF in H_2O, and the sample is placed in a metal sputtering deposition chamber, Perkin-Elmer model 2400. When the vacuum is better than $6x10^{-6}$ torr, argon gas is fed in to a pressure of 10 mtorr, and the

wafer is sputter metallized with 20 nm of Pd followed by 400 nm of Au on the implanted side. The wafer is now diced into 3 mm squares. The square is lapped with #1900 Al_2O_3 grit down to 70 microns thick on the non-metalized side. The sample is polished etched to 50 microns thick. The newly etched side is implanted with boron for a degenerate contact at $2x10^{13}$ cm^{-2} @ 33kV. The dose is low enough to allow illumination through the contact and with only a small fraction of the incoming IR photons absorbed. The contact absorbs about 20% of the photons in the 60 to 140 cm^{-1} range. See Appendix D. The device can be annealed at a temperature up to the Au-Ge eutectic temperature of 360°C, usually at 330°C for 1 hour in Ar. Annealing is required to removed deep level defects that might trap holes during operation. The front contact must be protected while the sides are etched to remove saw damage and because of stray ions from the implantation process that would increase the dark currents. Picene or protective wax is applied to define the front contact, the sample is polished etched again, and the wax is removed with solvent. The device is now ready for testing.

Appendix B: Fabrication of Planar Boron Implanted BIB Detector

Photolithography was done in the building 70A-3rd floor clean room operated by Jack Walton at Lawrence Berkeley Laboratory. To mask Ge for implantation, photoresist and photolithography are used to etch patterns into a silver layer on optically polished Ge.

An optically polished wafer of germanium was argon sputtered with 1 μm of Ag at 500W of forward power in a Perkin-Elmer 2400 metal sputterer. The coated wafer was then pre-baked at 140°C for at least 15 minutes to remove water from the surface, which would degrade the photoresist adhesion. The wafer was placed on a spinner and a positive photoresist, Microposit SPR2-1.3, was applied at 4500 rpm to form a 1 μm layer. The resist was soft baked at 90°C for 10 minutes to harden it for contact lithography. The wafer was centered in the Kaspar mask aligner and exposed with mask 1. Mask 1 was used to place alignment marks for dicing up devices and identifying contact pads to the devices. The resist was exposed for 10 seconds, developed for 40 seconds (Microposit MF322), and quenched in distilled water. The resist was then hardbaked for 30 minutes at 140°C, so it will withstand the Ag etch. The resist pattern was checked under the microscope for failures in resist adhesion and any particles. The pattern of mask 1 was replicated in the silver by etching for 6 seconds in 50% HNO_3 followed by quenching in distilled water. The pattern is then etched into the Ge using a solution of 30% H_2O_2 for 10 minutes at room temperature (~24nm/min at room temperature). The photoresist is removed with PRS2000 Positive Resist Stripper or acetone.

For the second lithography step positive photoresist was reapplied with the same conditions for the pre-bake and soft bake. Mask 2, for the contacts, was oriented to the

alignment marks previously etched into the Ag and Ge. The photoresist was exposed, developed, hardbaked, and examined under the microscope. The exposed Ag was etched in 50% nitric acid and the resist was removed. The exposed germanium surface was dipped in 5% HF in H_2O for 30 seconds, blown dry, and immediately placed in the implanter vacuum end station. Boron was implanted at 33 kV with a dose of $1x10^{14}$ cm^{-2} to form the contact.

The sample is returned to the clean room, and positive photoresist is applied with the same conditions of prebake and soft bake. Mask 3 delineates the infrared active absorbing region, must be oriented precisely (~1 μm) to the alignment marks from mask 2 for the device to work properly. The photoresist was developed and then hardbaked. The Ag was etched, the photoresist was removed, and the germanium was implanted again, but with much higher energies. The implant sequence was $1.8x10^{12}$ cm^{-2} at 400keV, $8.5x10^{11}$ cm^{-2} at 200 keV, $5.5x10^{11}$ cm^{-2} at 80 keV and $2x10^{11}$ cm^{-2} at 33keV. This series gives an approximate concentration of $3x10^{16}$ cm^{-3} to a depth of 1 μm. The 400 keV boron implant is done by implanting doubly-charged boron ($^{11}B^{++}$) with the voltage set at 200kV. To obtain the proper implant dose, the dosimeter must be set at twice the intended value of charge to compensate for the double charge of the ions. This implant step was time-consuming, due to the low concentration of doubly-charged ions in the source plasma of the ion implanter.

After implantation the silver was removed. The detector was cut out of the wafer, solvent cleaned, soaked in 10% KCN in H_2O, and annealed at 450°C for 2 hours in argon or N_2+4%H_2 gas. Wires are connected to the contacts with silver epoxy.

Appendix C: Phosphorus Implanted Contact in Ge

A phosphorus n^+ contact in Ge was characterized at various temperatures. A p-type germanium wafer was implanted with phosphorus to form a degenerately doped n^+ contact. By implanting phosphorus with a dose of $2x10^{14}$ cm^{-2} at 40kV and $4x10^{14}cm^{-2}$ at 75kV, into germanium at 104K, an amorphous layer is formed. This amorphous layer regrows with better crystalline quality and dopant activation than room temperature implanted layers.

The germanium crystal 822-15.1 was used with a shallow net acceptor concentration of 10^{11} cm^{-3}. The sides were etched with the implant protected. Metal was sputter deposited through a mask into 4 parallel strips, 20 nm Pd and 400 nm of Au. The sample was annealed with a temperature ramp of 50°C to 330°C in 15hrs in nitrogen gas. Current was passed through the outer 2 contacts and the voltage was measured on the inner two. Measurements were made at 3 temperatures: 300, 77, and 4.2K. Two point measurement were identical to the four point measurements. Results are shown in Fig. 1.

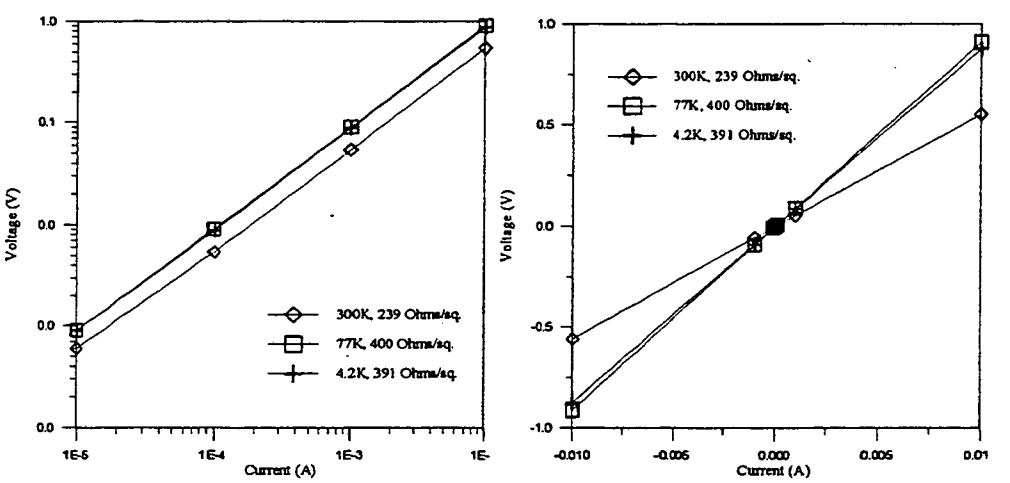

Fig. 1. Current-Voltage Characteristic of Phosphorus Contact.
(a) Log V- Log I, (b) V - I

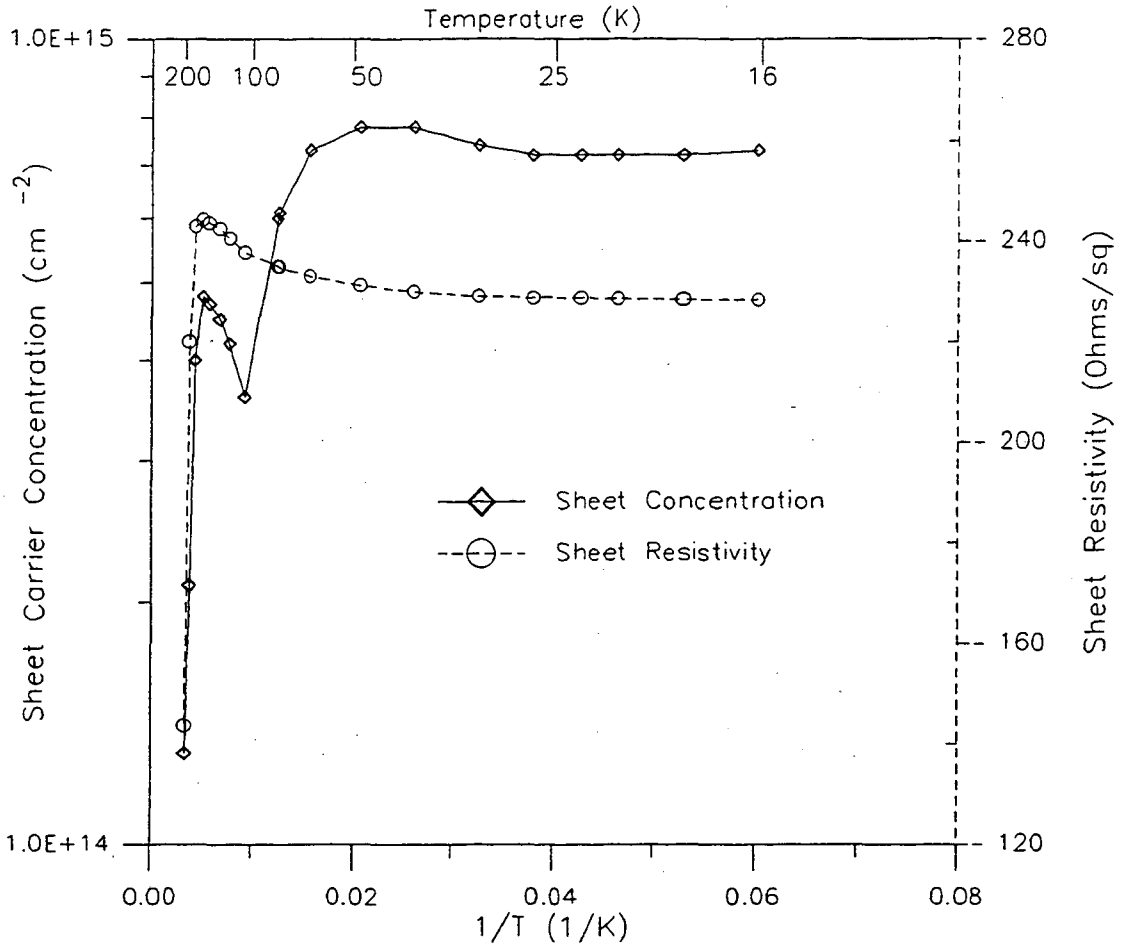

Fig. 2. Hall Effect on Phosphorus Implanted into p-Ge 822-15.1

Variable temperature Hall effect was performed on the phosphorus implanted layer, shown in Fig. 2. The beginning part of the Hall effect curve above 100 K is due to the structure of a 100 nm thick implanted layer on a p-type germanium substrate doped to approximately 10^{11} cm^{-3}. The substrate is intrinsic from 300 K to 200 K, so electrons in the substrate contribute. From 200 K to 100 K, the mobility in the substrate is much higher than the implanted layer, so it reduces the Hall voltage. Below 100K, a junction forms between the n layer and p substrate and isolates the layer. The electron concentration is independent of temperature as expected for a degenerate semiconductor.

Appendix D: IR Photon Absorption in Boron Implanted Contacts

The absorption of semi-transparent boron implanted contacts is an important detector parameter. Boron was implanted at 35kV at doses of $1x10^{14}$, $2x10^{13}$, and $2x10^{12}$ cm^{-2} into Ge#730 and annealed at 330°C for 2 hours. Absorption measurements were done at 2.0K with a stressed Ge:Ga detector, 1/2 mil beam splitter, and 23 Hz chopping frequency. The ratio of the transmission from the implanted samples was divided by an unimplanted reference sample and is shown in Fig. 3. The data shows Fabry-Perot oscillations in the transform, because the Ge wafers were plane parallel.

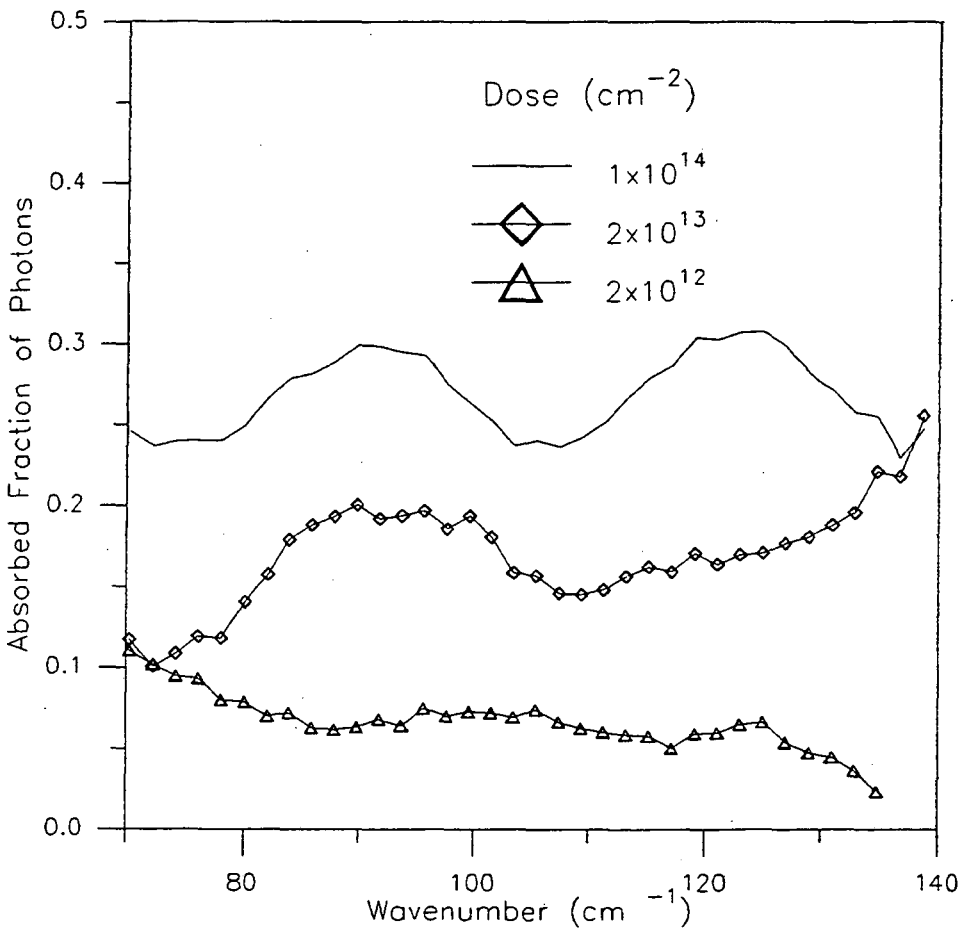

Figure 3. Fraction of absorbed photons by boron implanted contact

LAWRENCE BERKELEY LABORATORY
UNIVERSITY OF CALIFORNIA
TECHNICAL INFORMATION DEPARTMENT
BERKELEY, CALIFORNIA 94720